

# Where are the Luminous Red Galaxies (LRGs)? Using correlation measurements and lensing to relate LRGs to dark matter halos

Chiaki Hikage<sup>1</sup>, Rachel Mandelbaum<sup>2,3</sup>, Masahiro Takada<sup>4</sup>, and David N. Spergel<sup>2,4</sup>

<sup>1</sup> *Kobayashi Maskawa Institute (KMI), Nagoya University, Aichi 464-8602, Japan*

<sup>2</sup> *Department of Astrophysical Sciences, Princeton University, Peyton Hall, Princeton NJ 08544, USA*

<sup>3</sup> *Department of Physics, Carnegie Mellon University, Pittsburgh, PA 15213, USA*

<sup>4</sup> *Kavli Institute for the Physics and Mathematics of the Universe (Kavli IPMU, WPI), The University of Tokyo, Chiba 277-8582, Japan*

27 May 2022

## ABSTRACT

Nonlinear redshift-space distortions, the Finger-of-God (FoG) effect, can complicate the interpretation of the galaxy power spectrum. Here, we demonstrate the method proposed by Hikage et al. (2012) to use complimentary observations to directly constrain this effect on the data. We use catalogs of Luminous Red Galaxies (LRGs) and photometric galaxies from the Sloan Digital Sky Survey (SDSS) Data Release 7 (DR7) to measure the redshift-space power spectrum of LRGs, the cross-correlation of LRGs with the shapes of background photometric galaxies (galaxy-galaxy weak lensing), and the projected cross-correlation of LRGs with photometric galaxies having similar photometric redshifts to the LRG spectroscopic redshift. All of these measurements use a reconstructed halo field. While we use the position of each LRG for single LRG systems, we compare the measurements using different halo-center proxies for multiple-LRG systems (4.5 per cent of all the halos): the brightest LRG position (BLRG), the faintest LRG position (FLRG) and their arithmetical mean position (Mean), respectively, in each system. We find significant differences in the measured correlations of different centers, showing consistent off-centering effects in the three observables. By comparing the measurements with a halo model that treats the satellite photometric galaxies as being distributed according to a generalized NFW profile, we find that  $\sim 40$  (70) per cent of BLRGs (FLRGs) are off-centered satellite galaxies in the multiple-LRG systems. The satellite LRGs have typical off-centering radius of  $\sim 400$  kpc/ $h$ , and velocity dispersion of about 500 km/s in host halos with a mean mass of  $1.6 \times 10^{14} M_{\odot}/h$ . We show that, if LRGs in the single LRG systems have similar offsets, the residual FoG contamination in the LRG power spectrum can be significant at  $k \gtrsim 0.1$  h/Mpc, which may cause a bias in cosmological parameters determined by the shape of the power spectrum, such as the neutrino mass. Our results demonstrate that overlapping spectroscopic and imaging galaxy surveys can be used to observationally calibrate the FoG contamination and more robustly use the galaxy power spectrum for cosmological measurements.

**Key words:** cosmology: theory and observations – galaxy clustering – gravitational lensing: weak – large-scale structure of the Universe – cosmological parameters

## 1 INTRODUCTION

Large-scale structure surveys are one of the primary tools for studying the nature of dark matter, dark energy and the initial conditions in the early universe (Davis & Huchra 1982; de Lapparent et al. 1986; Kirshner et al. 1987; York et al. 2000b; Peacock et al. 2001). Over the coming decade, astronomers are embarking on even larger surveys including the Baryon Oscillation Spectroscopic Survey (BOSS<sup>1</sup>,

<sup>1</sup> <http://cosmology.lbl.gov/BOSS/>

Dawson et al. 2012), WiggleZ<sup>2</sup> (Blake et al. 2011), Vipers<sup>3</sup>, FMOS<sup>4</sup>, HETDEX<sup>5</sup>, BigBOSS<sup>6</sup> (Schlegel et al. 2009), Subaru Prime Focus Spectrograph (PFS<sup>7</sup>; Ellis et al. 2012), Euclid<sup>8</sup>, and WFIRST<sup>9</sup>. The upcoming generation of surveys is motivated by our desire to understand cosmic acceleration and to measure the composition of the universe by simultaneously measuring geometry and dynamics (Wang et al. 1999; Eisenstein et al. 1999; Tegmark et al. 2004; Cole et al. 2005). Measurements of the baryon acoustic oscillation (BAO) scale provide us with a robust geometrical probe of the angular diameter distance and the Hubble expansion rate (Eisenstein et al. 2005; Percival et al. 2007; Anderson et al. 2012). Observations of redshift-space distortion measure the growth rate of structure formation (Zhang et al. 2007; Guzzo et al. 2008; Wang 2008; Guzik et al. 2010; White et al. 2009; Percival & White 2009; Song & Percival 2009; Song & Kayo 2010; Yamamoto et al. 2010; Tang et al. 2011; Reid et al. 2012). Combining measurements of the geometry of the universe and the growth of structure formation provides a key clue to understanding the nature of dark energy as well as constraining properties of gravity on cosmological scales (Albrecht et al. 2006; Peacock et al. 2006).

If the distribution of galaxies in redshift space simply traced the underlying distribution of matter in real space, then cosmologists could easily interpret the large-scale structure observations. The universe, however, is not so simple: galaxies do not necessarily sit in the centers of dark matter halos and correspondingly, they are moving in these halos. This Finger-of-God (FoG) effect (Jackson 1972; Peacock & Dodds 1994; Scoccimarro 2004) is a significant source of systematic uncertainty in the cosmological interpretation of the redshift-space galaxy power spectrum

Reid et al. (2009) advocated using halos rather than Luminous Red Galaxies (LRGs; Eisenstein et al. 2001b) to mitigate FoG effects. In an analysis of LRGs from the Sloan Digital Sky Survey<sup>10</sup> (SDSS) Data Release 7 (DR7) catalog, Reid et al. (2010) implemented this scheme by removing satellite LRGs from within halos hosted by LRGs, with the aid of mock catalogs and the halo model prescription. Once such a halo catalog is constructed, the clustering properties of halos are easier to model, because halos have only bulk motions in large-scale structure, and therefore have a reduced FoG effect. However, even if one can perfectly choose one galaxy in each halo (e.g., the brightest LRG or the brightest cluster galaxy), there still remains uncertainty; the position of the chosen galaxy is not necessarily at the halo center (Skibba et al. 2011), and the off-centered galaxies have an internal motion relative to the true halo center, which causes residual FoG contamination (Seljak 2001; White 2001; Hikage et al. 2012).

In our previous paper (Hikage et al. 2012), we developed a method to correct the residual FoG effect by combining the redshift-space galaxy power spectrum with the cross-correlation of spectroscopic galaxies with images of background galaxies – the so-called galaxy-galaxy weak lensing (e.g., Mandelbaum et al. 2006b; Sheldon et al. 2009; Leauthaud et al. 2010; Okabe et al. 2010). The galaxy-galaxy lensing measures the average mass distribution around spectroscopic galaxies; i.e., at small scales, it reveals the mass profile of the halos hosting the lens galaxies, while on large scales it is sensitive to the mass distribution surrounding the host halos. However, if we include off-centered galaxies and use their positions as a proxy for the center of each halo, the lensing signals at angular scales smaller than the typical offset scale are diluted. In other words, comparing the galaxy-galaxy lensing signals of different halo-center proxies can be used to infer the amount of the off-centered galaxy contamination (Johnston et al. 2007; Leauthaud et al. 2010; Okabe et al. 2010; George et al. 2012, also see Oguri & Takada 2011 for a useful formulation of the off-centering effect on galaxy-galaxy weak lensing). Hence, a weak-lensing based calibration of the FoG effect in redshift-space power spectrum measurements can be feasible if spectroscopic and imaging surveys observe the same region of the sky. Fortunately, this is the case for many upcoming surveys: the BOSS and the Subaru Hyper Suprime-Cam (HSC) Survey<sup>11</sup> (Miyazaki et al. 2006), the Subaru PFS and HSC surveys (Subaru Measurements of Images and Redshifts: the SuMIRe project), Euclid and WFIRST or a combination of LSST (LSST Science Collaborations et al. 2009) with spectroscopic surveys.

The goal of this paper is to implement this method and to determine how LRGs are distributed in dark matter halos. For this paper, we use the SDSS DR7 catalog to constrain the fraction of off-centered LRGs and the amount of the residual FoG contamination in the LRG power spectrum measurement. We focus on systems that contain multiple LRGs in the same halo, defined based on the friend-of-friends algorithm (Reid & Spergel 2009; Reid et al. 2010). Then, we compare the redshift-space power spectra and the cross-correlations of LRGs with shapes of background photometric galaxies, measured using different halo-center proxies. Furthermore, we also use the projected cross-correlations of LRGs with photometric galaxies that have similar photometric redshifts to the LRG redshift, and then compare the measurements using different halo centers. We employ the following three proxies for the halo center: the brightest LRG position, the faintest LRG position, and the arithmetical mean position of LRGs (their center-of-mass position without any weighting) in each multiple-LRG system. We show that comparing the measurements to the halo model allows us to constrain the population of off-centered LRGs, the amount of off-centering effects, and the residual FoG contamination.

The structure of this paper is as follows. In Section 2, we develop a halo model to compute the redshift-space power spectrum, LRG-

<sup>2</sup> <http://wigglez.swin.edu.au/site/>

<sup>3</sup> <http://vipers.inaf.it/>

<sup>4</sup> <http://www.naoj.org/Observing/Instruments/FMOS/>

<sup>5</sup> <http://hetdex.org/>

<sup>6</sup> <http://bigboss.lbl.gov/>

<sup>7</sup> <http://sumire.ipmu.jp/pfs/intro.html>

<sup>8</sup> <http://sci.esa.int/euclid>

<sup>9</sup> <http://wfirst.gsfc.nasa.gov/>

<sup>10</sup> <http://www.sdss.org/>

<sup>11</sup> <http://www.naoj.org/Projects/HSC/index.html>

galaxy lensing and LRG-photometric galaxy cross-correlation including off-centering effects. In Section 3, we show the power spectrum, galaxy-galaxy lensing and the photometric galaxy cross-correlation measured from the SDSS DR7 catalog of LRGs and photometric galaxies, using the different halo-center proxies. Then we constrain the model parameters by comparing the halo model predictions to the measurements. Based on these findings, in Section 4, we discuss the residual FoG contamination in the LRG power spectrum, and its impact on cosmological parameters. Section 5 is devoted to discussion and conclusions. Unless explicitly stated otherwise, throughout this paper we assume a WMAP-normalized  $\Lambda$ CDM model as our fiducial cosmological model (Komatsu et al. 2009):  $\Omega_b h^2 = 0.0226$ ,  $\Omega_{\text{cdm}} h^2 = 0.1109$ ,  $\Omega_\Lambda = 0.734$ ,  $\tau = 0.088$ ,  $n_s = 0.963$ , and  $\sigma_8 = 0.817$ , where  $\Omega_b$ ,  $\Omega_{\text{cdm}}$  and  $\Omega_\Lambda$  are the energy density parameters of baryon, CDM and dark energy (the cosmological constant with  $w_0 = -1$  here),  $\tau$  is the optical depth to the last scattering surface, and  $n_s$  is the tilt of the primordial curvature power spectrum.

## 2 THE EFFECTS OF OFF-CENTERED LRGs ON THE GALAXY CLUSTERING AND WEAK LENSING CORRELATIONS

To constrain the radial distribution of LRGs within their host halos, we use three observables that can be measured from the SDSS DR7 data (Abazajian et al. 2009b): the angle-averaged, redshift-space power spectrum of LRGs, the weak lensing correlation of LRGs with background galaxy images, and the projected cross-correlation of LRGs with photometric redshift galaxies that have photo- $z$ 's similar to the LRG redshift. When computing these correlation functions, we use the same LRG catalog, but compare the correlation functions measured using different halo-center proxies (see below). Before describing the measurements, we first describe our halo model for the correlation functions, including the effect of off-centered LRGs (also see Oguri & Takada 2011; Hikage et al. 2012).

### 2.1 Connecting LRGs to halos and the radial offset distribution of LRGs

Weak lensing studies (e.g., Mandelbaum et al. 2006b; Johnston et al. 2007) and clustering analyses (Ross et al. 2007, 2008; Wake et al. 2008; Zheng et al. 2009; Reid & Spergel 2009; White et al. 2011) have shown that most LRGs reside in massive halos of a few  $\times 10^{13} M_\odot$ . While the typical massive halo contains only one LRG, about 5 per cent of LRGs are found to be satellite galaxies in a halo; there is a population of halos that contain multiple LRGs (Reid & Spergel 2009). Including these satellite galaxies in the correlation function measurements alters the clustering signals at small scales. This contribution complicates the estimation of cosmological parameters, because the small-scale signals involve complicated physical processes of galaxy formation/evolution that are still very challenging to accurately model. Hence, in this paper, we employ a method similar to that developed in Reid & Spergel (2009) to connect the distribution of LRGs to that of host halos by removing satellite LRGs from the catalog (see also Reid et al. 2010). In other words, we assume that we can identify one LRG (or one halo-center proxy) in each LRG system.

Since we are interested in the LRG-related correlation functions, which are statistical quantities, we need to model the *average* radial distribution of LRGs within host halos as a function of halo mass  $M$ :  $p_{\text{off}}(r)$ , which is normalized as  $4\pi \int_0^{r_{\text{vir}}} r^2 dr p_{\text{off}}(r) = 1$ . If LRGs are at the halo center,  $p_{\text{off}}(r) = \delta_D(r)/4\pi r^2$ . For off-centered LRGs, the Fourier transform of the radial profile is given as

$$\tilde{p}_{\text{off}}(k; M) = 4\pi \int_0^{r_{\text{vir}}} r^2 dr p_{\text{off}}(r) \frac{\sin kr}{kr}, \quad (1)$$

where we will often omit the halo mass dependence of  $p_{\text{off}}$  for notational simplicity. For central LRGs,  $\tilde{p}_{\text{off}}(k) = 1$ . In this paper, we assume for simplicity that offset LRGs follow a Gaussian distribution,  $p_{\text{off}}(r) \propto \exp[-r^2/2R_{\text{off}}^2]$ , and treat  $R_{\text{off}}$  as a free parameter to constrain from the measured correlation functions. However, the exact shape of the  $p_{\text{off}}(r)$  is less important than its characteristic width.

### 2.2 The FoG effect on the redshift-space power spectrum of LRGs

As we discussed in detail in Hikage et al. (2012), the major effect of off-centered LRGs on the angle-averaged, redshift-space power spectrum of LRGs is the nonlinear redshift-space distortion effect, the so-called Finger-of-God (FoG) effect. If an LRG is offset from the true halo center, the LRG should be in motion with respect to it. This internal motion within halos causes the FoG effect on the LRG power spectrum, and can occur even if selecting one LRG (or one center more generally) per halo, provided that the selected LRG or center is not the center of mass of the halo. By employing the halo model approach, we can model the redshift-space LRG power spectrum at a redshift  $z$  as

$$P_{s,\text{LRG}}(k, \mu) = \left[ \frac{1}{\bar{n}_{\text{LRG}}} \int dM \frac{dn}{dM} b(M) N_{\text{HOD}}(M) \tilde{p}_{s,\text{off}}(k, \mu; M) \right]^2 P_{s,m}^{\text{NL}}(k, \mu), \quad (2)$$

where  $\mu$  is the cosine of the angle between the line-of-sight direction and the wavevector  $\mathbf{k}$ , i.e.  $\mu \equiv k_{\parallel}/k$ ;  $dn/dM$  is the halo mass function of halos with mass  $M$  and at redshift  $z$ ;  $b(M)$  is the linear halo bias function;  $N_{\text{HOD}}(M)$  is the halo occupation distribution (HOD) specifying the probability that halos of mass  $M$  host LRGs ( $N_{\text{HOD}} \leq 1$  in our setting);  $\bar{n}_{\text{LRG}}$  is the mean number density of LRGs defined as  $\bar{n}_{\text{LRG}} \equiv \int dM (dn/dM) N_{\text{HOD}}(M)$ ;  $P_{s,m}^{\text{NL}}$  is the nonlinear redshift-space power spectrum of dark matter. The offset function  $\tilde{p}_{s,\text{off}}(k, \mu)$  is defined by convolving the real-space offset profile  $p_{\text{off}}$  (Eq. 1) with the velocity function along the line-of-sight direction via the virial theorem. See Hikage et al. (2012) for details. Although we employ the linear halo bias in the above equation, which is not a good

approximation for a high-precision measurement in the quasi-nonlinear scales (Baldauf et al. 2010), this is not crucial for the following results, because we will focus on fractional differences between the redshift-space power spectra of different halo center proxies, where the bias factor or the dark matter power spectrum cancel out in the fractional difference.

To make the model more general, we introduce an additional parameter  $q_{\text{cen}}$  ( $0 \leq q_{\text{cen}} \leq 1$ ) to represent the fraction of central LRGs among all the LRGs in the sample: the fraction of central LRGs is  $q_{\text{cen}}$ , while  $1 - q_{\text{cen}}$  is the fraction of satellite LRGs. In this case, we can model the resulting redshift-space power spectrum by replacing  $\tilde{p}_{s,\text{off}}$  in Eq. (2) as

$$\tilde{p}_{s,\text{off}}(k, \mu) \longrightarrow q_{\text{cen}} + (1 - q_{\text{cen}})\tilde{p}_{s,\text{off}}(k, \mu). \quad (3)$$

Here we assumed that, for the first term, the central galaxies have no FoG suppression, i.e. are at rest at the center of the host halo, so that their  $\tilde{p}_{s,\text{off}} = 1$ .

In this paper, we consider the angle( $\mu$ )-averaged power spectrum defined as

$$\bar{P}_{s,\text{LRG}}(k) = \int_{-1}^1 \frac{d\mu}{2} P_{s,\text{LRG}}(k, \mu). \quad (4)$$

For notational simplicity, we will hereafter omit the notation “-” of  $\bar{P}_{s,\text{LRG}}(k)$ .

### 2.3 The effect of off-centered LRGs on LRG-galaxy weak lensing

By cross-correlating the positions of LRGs with shapes of background galaxies, we can measure the average *dark matter* distribution around LRGs – the so-called LRG-shear cross-correlation or LRG-galaxy weak lensing (Mandelbaum et al. 2006b, 2012b). If we include off-centered LRGs in the analysis, they dilute the measured dark matter profile at scales smaller than the off-centering radius (Johnston et al. 2007; Oguri & Takada 2011; Hikage et al. 2012). Under the assumption that the dark matter halos are well-described by an NFW profile (Navarro et al. 1996) or some other parametrized profile, we can use the measured surface density profile to infer the distribution of off-centered halos.

For the observable of the LRG-galaxy weak lensing, we use the projected mass profile measured as a function of the projected radius:

$$\Delta\Sigma(R) \equiv \int \frac{k dk}{2\pi} C_{\Sigma g}(k) J_2(kR), \quad (5)$$

where  $J_2(x)$  is the 2nd-order Bessel function;  $R$  is the projected separation between LRG and background galaxy in units of the comoving scale;  $C_{\Sigma g}(k)$  is the angular power spectrum of the projected mass and LRG cross-correlation, and we give the power spectrum as a function of the wavenumber  $k$  for convenience in the rest of our discussion. Here the projected radius needs to be estimated from the observed angular separation for each LRG-galaxy pair on the sky:  $R = \chi\theta$ , where  $\chi$  is the comoving radial distance to each LRG. This conversion requires a redshift for each lens LRG, which is available from the SDSS DR7 catalog, and the assumption of a background cosmological model, for which we assume the WMAP cosmology (Komatsu et al. 2011). The  $R$ -average preserves the physical scales of host halos, such as the virial radius. On the other hand, if the cross-correlation is done in terms of the angular separation, then different scales are mixed for the halos at different redshifts, causing a smearing of the halo mass profile.

Employing the flat-sky approximation and the halo model, we can express the power spectrum  $C_{\Sigma g}(k)$  as a sum of the 1- and 2-halo terms:

$$C_{\Sigma g}(k) = C_{\Sigma g}^{1h}(k) + C_{\Sigma g}^{2h}(k). \quad (6)$$

The 1-halo term arises from the mass distribution within one halo that hosts LRGs and is the dominant contribution to the signal at small radii, while the 2-halo term arises from the mass distribution surrounding the host halos and is the dominant contribution at large radii. Using Limber’s approximation (Limber 1954), the 1- and 2-halo terms are given as

$$\begin{aligned} C_{\Sigma g}^{1h}(k) &\equiv \int d\chi f_{\text{LRG}}(\chi) \int dM \frac{dn}{dM} N_{\text{HOD}}^{\text{LRG}}(M; z) [M \tilde{u}_{\text{NFW}}(k; M, z) \tilde{p}_{\text{off}}(k; M) + m_{\text{sh,LRG}}], \\ C_{\Sigma g}^{2h}(k) &\equiv \int d\chi f_{\text{LRG}}(\chi) \left[ \int dM \frac{dn}{dM} b(M; z) N_{\text{HOD}}^{\text{LRG}}(M; z) \right] \bar{\rho}_{m0} P_m^L(k; z), \end{aligned} \quad (7)$$

where  $\tilde{u}_{\text{NFW}}(k; M, z)$  is the Fourier transform of an NFW profile with mass  $M$  at redshift  $z$ ;  $m_{\text{sh,LRG}}$  is a parameter representing the typical mass of a sub-halo hosting a satellite LRG;  $\bar{\rho}_{m0}$  is the mean mass density today; and  $P_m^L(k)$  is the linear mass power spectrum (see Hikage et al. 2012, for details). Our use of the mean mass density today ( $\bar{\rho}_{m0}$ ) rather than at the LRG redshift is due to our use of comoving units throughout this paper. The definition of the power spectra differs from the usual definition by a factor of  $\chi^{-2}$  (e.g. see Eqs. 24 and 25 in Hikage et al. 2012, for comparison), arising from the conversion  $R \leftrightarrow \theta$  discussed above. In the following analysis, we will focus on the galaxy-galaxy lensing correlations at scales up to a few Mpc, where the 1-halo term is dominant. However, as a conservative approach, we also include the 2-halo term treating the bias parameter as a free parameter, and then derive constraints on the off-centering parameters, marginalized over other parameter uncertainties. The function  $f_{\text{LRG}}(\chi)$  in Eq. (7) is the radial selection function of LRGs defined as

$$f_{\text{LRG}}(\chi) \equiv \frac{1}{\bar{n}_{\text{LRG}}^{2D}} S_{\text{LRG}}(z),$$

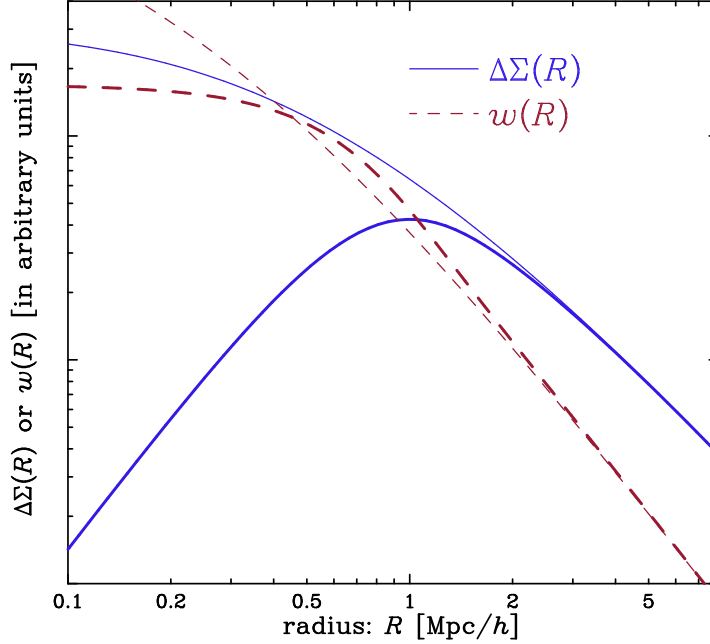


**Figure 1.** The plot demonstrates how the off-centering effect alters the LRG-galaxy weak lensing profile (solid curves) and the projected correlation function of LRGs with photometric galaxy positions (dashed) as a function of the projected radius from the true center or LRG positions, which are taken as the “center” in the correlation calculation for their respective thin and thick curves, respectively. The amplitude of each profile (in the  $y$ -axis) is plotted in arbitrary units. We assumed  $M_{180b} = 1.6 \times 10^{14} M_{\odot}/h$  and  $c_{180b} = 4.8$  for the halo mass and concentration parameters, respectively, and employed  $R_{\text{off}} = 400 \text{ kpc}/h$  for the off-centering parameter, where we assumed that all the LRGs are off-centered (see Eq. 1). The weak lensing distortion probes the gravitational tidal field around lensing halos and the cross-correlation of LRGs with galaxies probes the projected number density profile of galaxies in the host halos. The off-centering effect dilutes the correlation function amplitudes at radii smaller than the off-centering radius. However, note different features of the off-centering effects on the two profiles. For the projected correlation function, the off-centering effect causes an *enhancement* in the amplitude over a range of the intermediate radii;  $w_{\text{off}}(R) > w_{w/o \text{ off}}(R)$ . On the other hand, the inequality  $\Delta\Sigma_{\text{off}}(R) \leq \Delta\Sigma_{w/o \text{ off}}(R)$  always holds for the LRG-galaxy lensing profile due to the non-local nature of the tidal field.

$$\bar{n}_{\text{LRG}}^{2\text{D}} \equiv \int d\chi S_{\text{LRG}}(\chi) \int dM \frac{dn}{dM} N_{\text{HOD}}^{\text{LRG}}(M), \quad (8)$$

where  $S_{\text{LRG}}(z)$  is the redshift selection function of LRGs,  $\bar{n}_{\text{LRG}}^{2\text{D}}$  is the mean surface number density of LRGs, and the selection function satisfies the normalization condition  $\int d\chi f_{\text{LRG}}(\chi) \int dM (dn/dM) N_{\text{LRG}}(M) = 1$ . For simplicity, we assumed that the sub-halo lensing contribution can be characterized by a single number, a point mass, with a profile  $\Delta\Sigma(R) = m_{\text{sh,LRG}}/(\pi R^2)$ . See Section 3.2 in Takada & Jain (2003) for the conversion relation between the three-dimensional and projected mass density profiles in computing the projected power spectrum in a halo model formulation.

To gain insight into Eq. (7), let us consider a case that the LRGs are in a thin redshift slice centered at  $z_{\text{LRG}}$ , and reside in halos with a narrow mass range centered at  $\bar{M}$ . In this case, the power spectra can be simplified as

$$\begin{aligned} C_{\Sigma_g}^{1h}(k) &\simeq [\bar{M} \bar{u}_{\text{NFW}}(k; \bar{M}, z_{\text{LRG}}) \tilde{p}_{\text{off}}(k; \bar{M}) + m_{\text{sh,LRG}}], \\ C_{\Sigma_g}^{2h}(k) &\simeq b(\bar{M}) \bar{\rho}_{\text{m}0} P_m^L(k; z). \end{aligned} \quad (9)$$

These equations explicitly show that the 1-halo term arises from the NFW halo profile, and the 2-halo term probes the power spectrum with bias factor. When inverse Fourier-transforming the equations above, we can obtain the 1- and 2-halo term predictions for the projected mass profile  $\Delta\Sigma(R)$  to compare with the measurement. The above equations also show that the dimension of the power spectrum  $C_{\Sigma_g}(k)$  is in units of  $[M_{\odot}]$ ; the LRG-shear correlation is proportional to  $k^2 C_{\Sigma_g}(k)$  (see Eq. 5), which has dimensions of surface mass density in units of  $[M_{\odot}/\text{Mpc}^2]$ . Given statistical uncertainties of the measurements for a small sample size of the multiple-LRG systems, we will use the above equations to constrain the *averaged* halo parameters and off-center parameters for the multiple-LRG systems.

The thin and thick solid curves in Fig. 1 show how the off-centering effect dilutes the lensing profile. Here we only considered the 1-halo term, which is the dominant term on the small scales we are interested in. For model parameters, we assumed  $M_{180b} = 1.6 \times 10^{14} M_{\odot}/h$  and  $c_{180b} = 4.8$  for the halo mass and concentration parameters of an NFW profile, and employed  $R_{\text{off}} = 400 \text{ kpc}/h$  for the off-center profile parameter (see Eq. 1); these are typical values for multiple-LRG systems as we will find below. The off-centering effect dilutes the amplitude of lensing signal;  $\Delta\Sigma_{\text{off}}(R) < \Delta\Sigma_{w/o \text{ off}}(R)$  at radii smaller than the off-centering radius, and then  $\Delta\Sigma_{\text{off}}(R) = \Delta\Sigma_{w/o \text{ off}}(R)$  at larger radii. These features are useful in interpreting the lensing signals measured from the SDSS DR7 catalog.

When we consider the case that only some fraction of LRGs have offsets, and the remaining LRGs are central galaxies in their host halos, we replace the mass profile in the above equation with

$$\bar{M}\tilde{u}_{\text{NFW}}(k; \bar{M}, z_{\text{LRG}}) \tilde{p}_{\text{off}}(k; \bar{M}) \longrightarrow [q_{\text{cen}} + (1 - q_{\text{cen}})\tilde{p}_{\text{off}}(k; \bar{M})] \bar{M}\tilde{u}_{\text{NFW}}(k; \bar{M}, z_{\text{LRG}}), \quad (10)$$

where  $q_{\text{cen}}$  is the fraction of central LRGs in the sample, and we assumed that all the LRGs reside in halos of the same (or similar) mass scale  $\bar{M}$ . In this case, the sub-halo lensing contribution can be considered as the mean mass of sub-halos hosting the central and satellite LRGs. For the central LRGs, this enhancement relative to the NFW lensing of host halos might be considered to model additional lensing contribution due to baryonic contraction at the halo center. However, the sub-halo and baryonic contraction contributions are generally degenerate, unless we know which LRGs in the catalog are central galaxies. Hence the sub-halo contribution in the model (Eq. 9) can be considered as the average of the two effects.

## 2.4 The projected cross-power spectrum of off-centered LRGs with photometric galaxies

The third observable we consider is the projected cross-correlation function of LRGs with positions of photometric-redshift galaxies, measured as a function of the projected separation as in the LRG-galaxy weak lensing (see Eq. 5). Even in the presence of photometric redshift errors (photo- $z$  errors), the cross-correlation method is very powerful in a sense that it can *statistically* discriminate, from photo- $z$  outliers, photometric galaxies that actually cluster with LRGs at the same redshift<sup>12</sup> (Newman 2008). While including photo- $z$  outliers in the analysis dilutes the cross-correlation amplitude, it does not alter the shape of the correlation function.

Similar to the formalism for the LRG-galaxy lensing signal, the projected cross-correlation function can be expressed in terms of the power spectrum as

$$w_{gg}^{\text{cross}}(R) = \int \frac{kdk}{2\pi} C_{gg}^{\text{cross}}(k) J_0(kR), \quad (11)$$

where the notation ‘‘cross’’ is introduced to explicitly mean the cross-correlation between different populations of galaxies, spectroscopic LRGs and photometric galaxies, not the auto-correlation function of the same galaxy population. Based on the halo model, the galaxy power spectrum is given as  $C_{gg}^{\text{cross}}(k) = C_{gg}^{\text{cross},1h}(k) + C_{gg}^{\text{cross},2h}(k)$  with the 1- and 2-halo terms being defined as

$$\begin{aligned} C_{gg}^{\text{cross},1h}(k) &\equiv \int d\chi f_{\text{LRG}}(\chi) f_{\text{phg}}(\chi) \int dM \frac{dn}{dM} N_{\text{HOD}}^{\text{LRG}}(M) N_{\text{HOD}}^{\text{phg}}(M) \tilde{u}_{\text{NFW}}(k; M, z) \tilde{p}_{\text{off}}(k; M), \\ C_{gg}^{\text{cross},2h}(k) &\equiv \int d\chi f_{\text{LRG}}(\chi) f_{\text{phg}}(\chi) \left[ \int dM \frac{dn}{dM} N_{\text{HOD}}^{\text{LRG}}(M) b(M) \right] \left[ \int dM' \frac{dn}{dM'} N_{\text{HOD}}^{\text{phg}}(M') b(M') \right] P_m^L(k; z), \end{aligned} \quad (12)$$

where  $N_{\text{HOD}}^{\text{phg}}(M)$  is the halo occupation distribution for photometric galaxies, and we have assumed that the radial profile of photometric galaxies within the host halos follows an NFW profile for simplicity (see below for the analysis relaxing the assumption). We again note that, in the following results, we will focus on the cross-correlation at scales up to a few Mpc, so our use of the linear power spectrum in the 2-halo term does not cause any serious systematic error. We will take into account the uncertainty in the 2-halo term by treating the bias parameter as a free parameter, as in the LRG-galaxy lensing case. Taking into account the photo- $z$  errors, the redshift selection function  $f_{\text{phg}}$  is given as

$$f_{\text{phg}}(\chi) \equiv \frac{1}{\bar{n}_{\text{phg,all}}^{2\text{D}}} p(z|z_{\text{phz}}) \frac{dz}{d\chi}, \quad (13)$$

where  $p(z|z_{\text{phz}})\Delta z$  is the probability that photometric galaxies with photo- $z$  of  $z_{\text{phz}}$  have a true redshift in the range  $[z - \Delta z/2, z + \Delta z/2]$ . The probability satisfies the following normalization condition:  $\int dz p(z|z_{\text{phz}}) = 1$ . However, generally  $p(z|z_{\text{phz}})\Delta z \leq 1$  around the LRG redshift, so the factor  $p(z|z_{\text{phz}})\Delta z$  represents the dilution effect that is caused by including photo- $z$  outliers in the correlation analysis. The quantity  $\bar{n}_{\text{phg,all}}^{2\text{D}}$  is the mean surface number density of all the photo- $z$  galaxies, defined as  $\bar{n}_{\text{phg,all}}^{2\text{D}} \equiv \int d\chi p(z|z_{\text{phz}}) (dz/d\chi) \int dM (dn/dM) N_{\text{HOD}}^{\text{phg}}(M)$ . The selection function  $f_{\text{phg}}(\chi)$  satisfies the normalization condition:  $\int d\chi f_{\text{phg}}(\chi) \int dM (dn/dM) N_{\text{HOD}}^{\text{phg}}(M) = 1$ .

Assuming a thin redshift slice and narrow halo mass bin of LRGs, we can simplify the galaxy power spectra as

$$\begin{aligned} C_{gg}^{1h}(k) &\simeq \frac{1}{\Delta\chi \left. \frac{dn}{dM} \right|_{M=\bar{M}} \Delta M} \frac{\bar{n}_{\text{phg}}^{2\text{D}}(z_{\text{LRG}})}{\bar{n}_{\text{phg,all}}^{2\text{D}}} \tilde{u}_{\text{NFW}}(k; \bar{M}, z_{\text{LRG}}) \tilde{p}_{\text{off}}(k; \bar{M}), \\ C_{gg}^{2h}(k) &\simeq \frac{1}{\Delta\chi} \frac{\bar{n}_{\text{phg}}^{2\text{D}}(z_{\text{LRG}})}{\bar{n}_{\text{phg,all}}^{2\text{D}}} \bar{b}_{\text{LRG}} \bar{b}_{\text{phg}} P_m^L(k; z_{\text{LRG}}), \end{aligned} \quad (14)$$

where  $\Delta\chi$  is the radial distance width of the LRG distribution, and  $\bar{n}_{\text{phg}}^{2\text{D}}(z_{\text{LRG}})$  is the average surface number density of photometric galaxies that indeed lie in the LRG redshift bin and reside in halos hosting LRGs, defined as  $\bar{n}_{\text{phg}}^{2\text{D}}(z_{\text{LRG}}) \equiv p(z_{\text{LRG}}|z_{\text{phz}}) dz/d\chi|_{z_{\text{LRG}}} \Delta\chi dn/dM|_{\bar{M}} \Delta M$ . The dimension of the power spectra is  $[\text{Mpc}]^2$ . The prefactor  $\bar{n}_{\text{phg}}^{2\text{D}}(z_{\text{LRG}})/\bar{n}_{\text{phg,all}}^{2\text{D}}$  gives the fraction of photometric galaxies with true redshifts that are sufficiently close to the LRG redshift. Hence, this factor accounts for the dilution effect due to photo- $z$  outliers that we include

<sup>12</sup> At small scales where lensing magnification is important, there might seem to be some additional clustering with photometric galaxies; this should also be modeled if those scales are used for the measurements (unlike in this work).

in our sample. Also note that the 1-halo term of the power spectrum behaves like the Poisson shot noise  $1/[\Delta\chi(dn/dM)\Delta M]$  in the limits of  $\tilde{p}_{\text{off}}, \tilde{u}_{\text{NFW}} \rightarrow 1$ , where  $\Delta\chi(dn/dM)\Delta M$  is the mean surface number density of halos hosting LRGs. In the following analysis, we introduce a nuisance parameter to model the amplitude uncertainty, and will derive constraints on the off-centering profile of LRGs, marginalizing over the nuisance parameter.

The dashed curves in Fig.1 demonstrate the off-centering effect on the projected correlation function. The off-centering effect dilutes the amplitude at small radii,  $w_{\text{off}}(R) < w_{w/o \text{ off}}(R)$ , however it *enhances* the amplitude at the intermediate radii,  $w_{\text{off}}(R) > w_{w/o \text{ off}}(R)$ . Then the two correlation functions with and without the off-centering effect agree at the larger radius. The enhancement in the correlation amplitude is contrasted to the off-centering effect on the LRG-galaxy lensing profile, which probes the non-local tidal field around the LRG halos. Here, although we assume that the photometric galaxies follow an NFW profile for simplicity, these qualitative features are still present for any arbitrary profile of the projected density field. These features are useful when making an interpretation of the measured cross-correlation functions for the SDSS DR7 data as we will show below.

When further including the mixture of central and satellite LRGs in the sample, we will use the replacement given in Eq. (10) to model the power spectrum  $C_{gg}(k)$ . Fourier-transforming the above equations gives the halo model predictions for the projected cross-correlation  $w^{\text{cross}}(R)$  to compare with the measurement. We will use the above equations to derive the *averaged* halo parameters and off-centering parameters in the following analysis.

It is important to note that while the prediction for the LRG-photometric galaxy cross-correlation function on small scales includes a convolution of the radial distribution of satellite galaxies with the off-centering distribution of our chosen halo centers, the power of this method is really in a comparison of results with *different* centers for the same halo and photometric galaxy catalogs. In this case, the radial distribution of satellite galaxies must be the same for all measurements, and only the off-centering distribution can cause differences between the measurements.

### 3 MEASUREMENTS AND RESULTS

#### 3.1 SDSS DR7 LRG Catalog

Here we describe the data used for the analysis in this paper, all of which come from the Sloan Digital Sky Survey Data Release 7 catalog (SDSS DR7). The SDSS (York et al. 2000a) imaged roughly  $\pi$  steradians of the sky, and followed up approximately one million of the detected objects spectroscopically (Eisenstein et al. 2001a; Richards et al. 2002; Strauss et al. 2002). The imaging was carried out by drift-scanning the sky in photometric conditions (Hogg et al. 2001; Ivezić et al. 2004), in five bands (*ugriz*; Fukugita et al. 1996; Smith et al. 2002) using a specially-designed wide-field camera (Gunn et al. 1998). These imaging data were used to create star and galaxy catalogs that we use in this paper. All of the data were processed by completely automated pipelines that detect and measure photometric properties of objects, and astrometrically calibrate the data (Lupton et al. 2001; Pier et al. 2003; Tucker et al. 2006). The SDSS I/II imaging surveys were completed with a seventh data release (Abazajian et al. 2009a), though this work will rely as well on an improved data reduction pipeline that was part of the eighth data release, from SDSS III (Aihara et al. 2011); and an improved photometric calibration ('ubercalibration', Padmanabhan et al. 2008).

We use the SDSS DR7 LRGs in the Northern Galactic Cap with a contiguous region, which is made publicly available by Kazin et al. (2010). The sample consists of 96,762 LRGs with absolute magnitude  $-23.2 < M_g < -21.2$  in the redshift range  $0.16 < z < 0.47$  covering about  $1.58 (\text{Gpc}/h)^3$  comoving volume in the concordance  $\Lambda\text{CDM}$  model, with nearly constant comoving number density for  $z < 0.36$  and decreasing number density above that redshift. To recover the halo density field from the LRG distribution, we used the Counts-in-Cylinders (CiC) techniques developed by Reid & Spergel (2009) to identify groups of  $N_{\text{LRG}} \geq 2$  LRGs occupying the same halo. To be more precise, multiple LRGs are considered as neighbors of the same group when the transverse separation satisfies  $\Delta r_{\perp} \leq 0.8h^{-1}\text{Mpc}$  and the redshift difference satisfies  $\Delta z/(1+z) \leq 0.006$  corresponding to  $\delta v_p = 1800 \text{ km/s}$ . The radial-direction length of the cylinder is motivated by the virial motion of galaxies in a massive halo, and was shown to safely include satellite galaxies in the same halo using mock catalogs (Reid et al. 2009). Then LRGs in different CiC groups are grouped together by a Friends-of-Friends method (by connecting any of the member galaxies in the different CiC cylinders). Table 1 summarizes the reconstructed LRG groups. The total number of halos inferred from the LRG catalog is 92,046, and about 4.5 per cent are multiple-LRG systems. Among the multiple-LRG systems, about 90 per cent are systems with two LRGs ( $N_{\text{LRG}} = 2$ ). We also generate random catalogs that have the same area coverage and redshift distribution as the halos; these are used to estimate the LRG-galaxy lensing signal and the cross-correlation with photometric galaxies in the imaging data.

Although this CiC method was carefully studied in Reid & Spergel (2009), it might provide an imperfect catalog of LRG-host halos; for example, single-LRG systems might be in multiple LRG-systems, if other LRG candidate(s) lack(s) spectra due to fiber collisions. However, given the different goal of this work, we do not explore a modification of the CiC method. Rather, we will focus on a possible residual contamination of off-centered LRGs and discuss the impact on the LRG clustering analysis, by using the same method of halo reconstruction in the previous study. The off-centering effect or the offset of LRGs from the true center of dark matter halo is very difficult to observationally constrain, and we hope our method gives a way to observationally constrain the off-centering effect.

To compute the power spectrum and the cross-correlations from the LRG-inferred halos, we must define the halo center for each LRG system. (1) For single LRG systems with  $N_{\text{LRG}} = 1$ , we use the redshift and angular position of LRG as the halo center proxy. (2) For multiple-LRG systems with  $N_{\text{LRG}} \geq 2$ , we use the following three halo center proxies in order to compare the measurements:

Number of LRG(s) ( $N_{\text{LRG}}$ ) in each FoF group	Number of LRG FoF groups (fraction)
1	87889 (95.5 per cent)
2	3713
3	358
4	65
5	14
6	6
7	1
Total	92046 (100 per cent)

**Table 1.** The number of different LRG groups after the CiC-FoF based group finder of the SDSS DR7 LRG distribution. “ $N_{\text{LRG}} = 1$ ” means single LRG systems, where each region has a single LRG in the cylinder region in angular and redshift space. “ $N_{\text{LRG}} \geq 2$ ” systems are multiple-LRG systems, where each region contains  $N_{\text{LRG}}$  LRGs in the cylinder region.

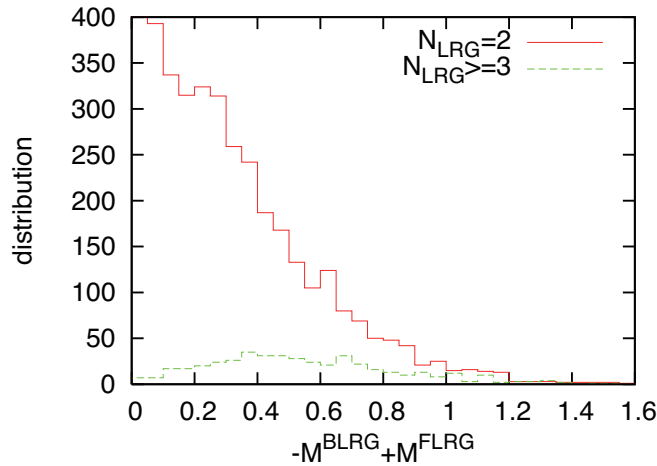


**Figure 2.** The histogram of magnitude differences between the brightest and faintest LRGs (BLRG and FLRG) in multiple-LRG systems (see Table 1). The solid-line histogram is for the systems having 2 LRGs inside, while the dashed line is for the systems with  $N_{\text{LRG}} \geq 3$ .

- *BLRG*: the brightest LRG (BLRG) in each multiple-LRG group as the halo center. The BLRG is expected to reside in the most massive sub-halo and therefore be closer to the underlying true center due to dynamical friction theory.
- *FLRG*: the faintest LRG (FLRG) as the halo center; it can be considered as the extreme counterpart to BLRG.
- *Mean*: the mean position of LRGs in their redshift and angular positions. Note that we did not use any luminosity or other weighting to estimate the mean position. This is the halo-center proxy used in Reid et al. (2010).

Fig.2 shows the distribution of magnitude difference between the brightest and faintest LRGs (BLRG and FLRG) in the multiple-LRG systems. The magnitude difference is typically within 1 mag. Most of the 2-LRG systems have a magnitude difference that is less than a few tenths of a magnitude, implying that the BLRG and FLRG are not very different, and the FLRG may be closer to the true center than the BLRG in some halos, as we will address below.

### 3.2 LRG power spectrum

We first use the angle-averaged, redshift-space power spectrum of LRG-inferred halos to study the effect of off-centered LRGs. We employed the method of Reid et al. (2010) to measure the power spectrum from the reconstructed halo density field, as briefly summarized below.

The power spectrum measurement was done using the Fourier decomposition method developed in Feldman et al. (1994). We used  $1024^3$  grids in a cubic box with side length 2.6 Gpc/h, which covers the entire region of the LRG distribution in redshift space. The density fluctuation field of halos on a grid is estimated by placing the halos onto the grid and subtracting an unclustered “random” catalog, which matches the halo selection. The random catalog is given from Kazin et al. (2010), where the variations in angular and radial selections and the effect of fiber collisions are taken into account. In doing the density assignment from the LRG-halos or random catalogs, we used the weighting method in Percival et al. (2004) using a luminosity-dependent bias model. However, note that we used the luminosity of BLRG in each halo to compute the weighting, and used the *same* weight for all the three BLRG, FLRG and Mean centers in the multiple-LRG systems. Thus we used the *same* random catalogs and the *same* luminosity weights for all the three BLRG-, FLRG- and Mean-center catalogs in order to avoid any unwanted effect on the measured power spectra. We also note that, in the following results, we focus on relative *differences*



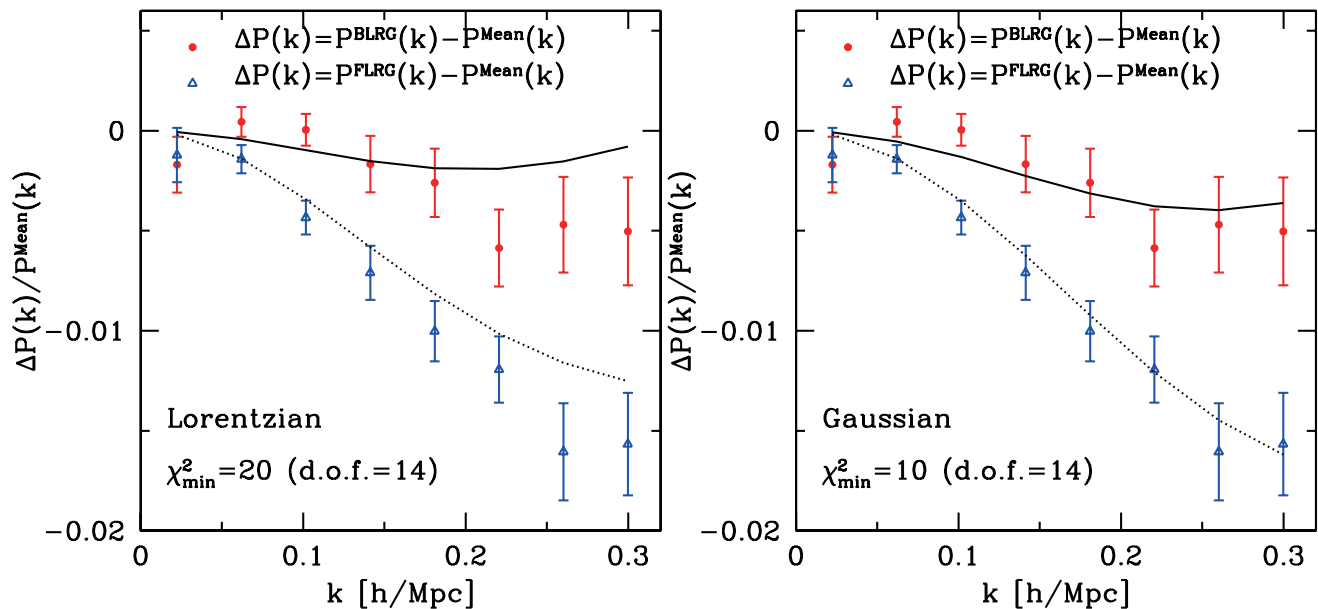


**Figure 3.** The angle-averaged redshift-space power spectra for the LRG-inferred halos, measured using the different halo center proxies for the multiple-LRG systems: the brightest LRG position (BLRG), the faintest LRG position (FLRG) and the mean position (Mean) of LRG positions in angular and redshift space (see Section 3.1 for the details). The circle and triangle symbols show the fractional differences of the halo power spectra of the BLRG or FLRG centers, respectively, relative to the spectrum of the Mean center. Since we used the same halos and power spectrum measurement methods, the difference arises solely from the different halo centers of the multiple-LRG systems. The FLRG power spectrum shows a larger suppression compared to the other two, which indicates that the FLRGs have the largest offsets and thus largest internal velocity dispersion in the multiple-LRG systems. The BLRG power spectrum still shows some suppression compared to that for the Mean, which indicates a residual off-centered effect of BLRGs. The solid and dashed curves in each panel show the best-fit FoG model assuming the Lorentzian (*left panel*) and Gaussian (*right panel*) functional forms. Note that the measurement points are the same in both panels.

between the measured power spectra and cross-correlation functions using the different centers, where the differences should not be sensitive to any details of the measurement methods.

To estimate the error bars or measurement uncertainties, we divide the LRG sample into 100 equal-area, nearly contiguous regions on the sky, and carry out the measurements of the LRG-inferred power spectra from each of those 100 regions (Mandelbaum et al. 2012b, hereafter M12); for some description of the limitations of bootstrap and jackknife resampling, see, e.g., Hartlap et al. (2007) and Hirata et al. (2004). Then we estimate the covariance matrix from the 100 power spectra. The jackknife resampling assumes independence of the regions, and thus cannot be used to obtain the error bars for scales comparable to the size of the regions (which are far larger than the maximum scales used for our fits).

Fig. 3 shows the measured power spectra of halos reconstructed from the SDSS LRG catalog. Plotted here is the fractional difference of the power spectra, measured by using either BLRG- or FLRG-halo centers, relative to the power spectrum calculated using the Mean-center in the multiple-LRG systems. The error bars at each  $k$  bin are estimated from the jackknife method we described above. Note that, in this analysis, we changed the redshift- and angular positions only for 4.5 per cent of the halos (the other 95.5 per cent are exactly the same since they include only single-LRG systems). The figure clearly shows that the power spectra calculated using both the BLRG and FLRG centers show smaller amplitudes with increasing  $k$  than the power spectrum calculated using the Mean center, implying that the BLRG and FLRG results are more affected by the FoG effect, leading to a stronger suppression in the power than the Mean spectrum. The significance of the differences is  $\Delta\chi^2 = 69, 120$  and  $138$  for the BLRG, FLRG and the combined BLRG and FLRG difference, respectively, corresponding to about  $8.2, 10.9,$  and  $11.7\sigma$  detections of the FoG effects, respectively. In these estimates, we included the correlations between the error bars at different  $k$  bins (which are typically around 0.1, but occasionally as large as 0.5), and the (significant) correlation between the BLRG and FLRG spectra using the full jackknife covariance matrix. The FLRG spectrum has more suppressed power, which is expected since fainter galaxies are more likely to be satellites, but it is more surprising that the BLRG power spectrum also shows the FoG suppression. This suggests that the BLRGs also have an off-centered distribution in the host halos, or some of the BLRGs are satellite galaxies. On the other hand, the power spectrum of the Mean center turns out to be least affected by the FoG effect, which is counter-intuitive, because there is no LRG at the inferred position. However, we note that most of the multiple-LRG systems have  $N_{\text{LRG}} = 2$  and a small magnitude difference between the two LRGs. Hence, some FLRGs, rather than the BLRGs, may be central galaxies in some of the host halos.

Following the method developed in Hikage et al. (2012), we can make a model interpretation of the measured power spectra for the different LRG-inferred halo centers. The redshift-space power spectrum we measure arises from auto- and cross-correlations of/between the single- and multiple-LRG halos, where the fraction of multiple-LRG halos among all the LRG-inferred halos is only 4.5 per cent, which we hereafter refer as  $f_{\text{M-LRG}} \equiv 0.045$ . We assume that only some fraction of the chosen LRGs are central galaxies in the single- or

multiple-LRG systems, and represent these fractions as  $q_{\text{cen}}^{\text{S-LRG}}$  or  $q_{\text{cen}}^{\text{M-LRG}}$  (to be more precise, we will consider  $q_{\text{cen}}^{\text{BLRG}}$  or  $q_{\text{cen}}^{\text{FLRG}}$  for the multiple-LRG halos, because we chose the galaxies for the halo center proxies). The remaining galaxies, given by  $(1 - q_{\text{cen}})$ , are satellites that cause the FoG effect. Including the parameter  $q_{\text{cen}}$  gives a better agreement with measurements of the LRG-galaxy lensing and the projected cross-correlation function of LRG-halos and photo- $z$  galaxies, to be described in subsequent sections. Thus, we can model the redshift-space power spectrum of the LRG-inferred halos as

$$P_s(k, \mu) = [1 + \beta\mu^2]^2 \left[ \bar{b}_{\text{S-LRG}}(1 - f_{\text{M-LRG}}) \left\{ q_{\text{cen}}^{\text{S-LRG}} + (1 - q_{\text{cen}}^{\text{S-LRG}}) \sqrt{F_{\text{S-LRG}}(k, \mu)} \right\} + \bar{b}_{\text{M-LRG}} f_{\text{M-LRG}} \left\{ q_{\text{cen}}^{\text{M-LRG}} + (1 - q_{\text{cen}}^{\text{M-LRG}}) \sqrt{F_{\text{M-LRG}}(k, \mu)} \right\} \right]^2 P_m^{\text{NL}}(k), \quad (15)$$

where  $\bar{b}_{\text{S-LRG}}$  and  $\bar{b}_{\text{M-LRG}}$  are the average bias parameters for the single- and multiple-LRG host halos, respectively;  $q_{\text{cen}}^{\text{S-LRG}}$  is the fraction of central LRGs in the single-LRG systems;  $q_{\text{cen}}^{\text{M-LRG}}$  is the fraction of either BLRGs or FLRGs to be centrals in the multiple-LRG systems. We have assumed that the redshift-space distortion effect due to the peculiar velocity field of halos is given by the Kaiser formula (Kaiser 1987), given by the function  $[1 + \beta\mu^2]^2$ , and  $\beta \equiv (1/b)d \ln D/d \ln a$  ( $D$  is the linear growth rate).  $P_m^{\text{NL}}(k)$  is the real-space, nonlinear power spectrum of dark matter, and  $F(k, \mu)$  is the velocity function to model the average velocity distribution of off-centered (satellite) LRGs within the host halos (see below). The coefficients  $(1 - f_{\text{M-LRG}})$  and  $f_{\text{M-LRG}}$  are the fractions of the single- and multiple-LRG halos relative to all the LRG-host halos, respectively. In the above equation, we assumed that the central LRG rests at the center of the host halo and therefore has no FoG effect. Thus, different populations of LRG-host halos (the single- and multiple-LRG systems in our case) cause FoG effects on the redshift-space power spectrum in different ways, varying with their fractions, the halo bias parameters and the fractions of satellite LRGs in each population. To compute the bias parameters, for simplicity we employ the halo bias using the average halo masses measured from the LRG-galaxy weak lensing for the assumed fiducial cosmology:  $\bar{M}_{\text{S-LRG}} = 0.4 \times 10^{14} M_{\odot}/h$  and  $\bar{M}_{\text{M-LRG}} = 1.6 \times 10^{14} M_{\odot}/h$ , respectively, estimated using the bias model in Sheth & Tormen (1999)<sup>13</sup>. For the velocity function  $F$ , we assume the following functional forms that are often used in the literature (Hamilton 1998):

$$F(k, \mu) = \begin{cases} \frac{1}{[1 + (k\mu\sigma_{v,\text{off}}/aH(z))^2]}, & \text{(Lorentzian FoG effect)} \\ \exp[-(k\mu\sigma_{v,\text{off}}/aH(z))^2], & \text{(Gaussian FoG effect)} \end{cases} \quad (16)$$

where  $\sigma_{v,\text{off}}$  is the typical velocity dispersion of off-centered LRGs. Note that “ $\sqrt{F}$ ” of  $\sqrt{F}$  in the FoG effect of Eq. (15) was introduced because the above functions are conventionally used to model the FoG effect on correlations between *two* satellite galaxies. Thus Eq. (15) is different from the form used in the literature, and predicts a non-trivial scale dependence as a function of wavenumber; e.g., at the large- $k$  limit, the FoG function asymptotically approaches a constant value,  $[\bar{b}_{\text{S-LRG}}(1 - f_{\text{M-LRG}})q_{\text{cen}}^{\text{S-LRG}} + \bar{b}_{\text{M-LRG}} f_{\text{M-LRG}} q_{\text{cen}}^{\text{M-LRG}}]^2$ , while the standard FoG function  $F \rightarrow 0$ .

The fractional power spectra shown in Fig.3 are with respect to the power spectrum for the “Mean” centers in the multiple-LRG systems. Hence we need to model the power spectrum for the Mean center based on our method. Fig.3 implies that the Mean centers, the mean position of BLRG and FLRG in multiple-LRG systems, are statistically closer to the true centers, such that the power spectrum is least affected by the FoG effect. Physically, this is very difficult to imagine, since we expect that the Mean center, which has no corresponding galaxy at the position, should be offset from the halo center to some degree. To consider the offset probability of the Mean centers, we need to include three cases: (1) within the host halo, BLRG is a central galaxy, while FLRG is a satellite galaxy, (2) FLRG is central, while BLRG is satellite, and (3) both BLRG and FLRG are satellites in their host halo. Among all the multiple-LRG systems, the probabilities of these 3 cases are given by  $q_{\text{cen}}^{\text{BLRG}}$ ,  $q_{\text{cen}}^{\text{FLRG}}$  and  $1 - q_{\text{cen}}^{\text{BLRG}} - q_{\text{cen}}^{\text{FLRG}}$ , respectively. With these in mind, the velocity dispersion of the Mean center can be estimated as

$$\begin{aligned} (\sigma_{v,\text{off}}^{\text{Mean}})^2 &= q_{\text{cen}}^{\text{BLRG}} \frac{(\sigma_{v,\text{off}}^{\text{FLRG}})^2}{4} + q_{\text{cen}}^{\text{FLRG}} \frac{(\sigma_{v,\text{off}}^{\text{BLRG}})^2}{4} + (1 - q_{\text{cen}}^{\text{BLRG}} - q_{\text{cen}}^{\text{FLRG}}) \frac{(\sigma_{v,\text{off}}^{\text{BLRG}})^2 + (\sigma_{v,\text{off}}^{\text{FLRG}})^2}{4} \\ &= \frac{(1 - q_{\text{cen}}^{\text{BLRG}}) (\sigma_{v,\text{off}}^{\text{BLRG}})^2 + (1 - q_{\text{cen}}^{\text{FLRG}}) (\sigma_{v,\text{off}}^{\text{FLRG}})^2}{4}, \end{aligned} \quad (17)$$

where the three terms in the first line correspond to the three cases mentioned above, and we have assumed no correlation between the distributions of BLRG and FLRG in each host halo as well as no correlation between the distributions of LRGs in different halos. We also assumed that BLRG and FLRG determine the mean position of LRGs in multiple-LRG systems, which may host more than two LRGs ( $N_{\text{LRG}} \geq 3$ ). Or equivalently we assumed that the Mean centers are determined mainly by the multiple-LRG systems with 2 LRGs, because the systems with 2 LRGs are a dominant population of the multiple-LRG systems (see Table 1). Thus we expect that the Mean centers always have offsets from the true center. The factor of 4 in the denominator of each term is from the fact that we computed the dispersion of

<sup>13</sup> While we have used a theoretical bias vs. halo mass relation, it is worth noting that the large-scale biases for LRG samples that together compose the LRG sample in this work were found (via direct-fitting to large-scale clustering and lensing measurements) to be  $2.07 \pm 0.05$  and  $2.26 \pm 0.06$  (Mandelbaum et al. 2012b). Thus we expect that the average of  $\bar{b}_{\text{S-LRG}}$  and  $\bar{b}_{\text{M-LRG}}$  (weighted by the relative fractions of single- and multiple-LRG systems) to lie in between those two measurements, which is indeed the case given the predominance of single-LRG systems. This confirms that use of these theoretical predictions is consistent with the data.

the off-centering amount of the Mean centers. For instance, in the first case (the first term in the above equation), suppose the line-of-sight displacement vector for the Mean center with respect to the true center in each system is defined as  $\vec{\delta}r_{\parallel, \text{Mean}} = \vec{\delta}r_{\parallel, \text{FLRG}}/2$  as the BLRG is at the halo center ( $\vec{\delta}r_{\parallel, \text{BLRG}} = 0$ ). Then the average  $\langle \vec{\delta}r_{\parallel, \text{Mean}} \rangle = 0$  and the dispersion  $(\sigma_{\text{off}}^{\text{Mean}})^2 = \langle (\vec{\delta}r_{\parallel, \text{Mean}})^2 \rangle = (\sigma_{\text{off}}^{\text{FLRG}})^2/4$ , yielding the factor of 4.

Hence, the fractional power spectrum shown in Fig.3 can be modeled based on our method, e.g. for the BLRG center, to first order in  $f_{\text{M-LRG}}$ :

$$\frac{\bar{P}_s^{\text{BLRG}}(k)}{\bar{P}_s^{\text{Mean}}(k)} - 1 \simeq 2f_{\text{M-LRG}} \left( \frac{\bar{b}_{\text{M-LRG}}}{\bar{b}_{\text{S-LRG}}} \right) \frac{\int_{-1}^1 \frac{d\mu}{2} (1 + \beta\mu^2)^2 \left[ q_{\text{cen}}^{\text{BLRG}} + (1 - q_{\text{cen}}^{\text{BLRG}}) \sqrt{F(k, \mu; \sigma_{v, \text{off}}^{\text{BLRG}})} - \sqrt{F(k, \mu; \sigma_{v, \text{off}}^{\text{Mean}})} \right]}{\int_{-1}^1 \frac{d\mu}{2} (1 + \beta\mu^2)^2}. \quad (18)$$

Thus the quantities such as  $P^{\text{NL}}(k)$  (or  $\beta$  to a good approximation) cancel out in the fractional difference, and the ratio of bias parameters ( $\bar{b}_{\text{M-LRG}}/\bar{b}_{\text{S-LRG}}$ ) is relevant. In the above equation, we also assumed that the FoG effect for the single-LRG systems is negligible, because the halos have a higher fraction of the central LRGs ( $q_{\text{cen}}^{\text{S-LRG}} \simeq 0.8$ ) and a smaller velocity dispersion due to the smaller halo mass as we will show in the following. Since  $\sigma_{v, \text{off}}^{\text{Mean}}$  is given in terms of  $\sigma_{v, \text{off}}^{\text{BLRG}}$  and  $\sigma_{v, \text{off}}^{\text{FLRG}}$  (and we have fixed the background cosmological model to compute the linear Kaiser factor  $\beta$ ), the relevant fitting parameters are 4:  $q_{\text{cen}}^{\text{BLRG}}$ ,  $q_{\text{cen}}^{\text{FLRG}}$ ,  $\sigma_{v, \text{off}}^{\text{BLRG}}$ , and  $\sigma_{v, \text{off}}^{\text{FLRG}}$ , respectively.

The solid and dotted curves in the left- and right-panels of Fig.3 show the best-fit FoG effect for the Lorentzian or Gaussian FoG models, respectively. In this fitting, for simplicity, we assumed that the fraction of central BLRGs or central FLRGs is  $q_{\text{cen}}^{\text{BLRG}} = 0.54$  or  $q_{\text{cen}}^{\text{FLRG}} = 0.32$ , respectively, as implied from the measurements of the LRG-shear lensing and the LRG-photo- $z$  galaxy cross-correlation in the subsequent sections. We find that the best-fit velocity dispersions for the satellite BLRGs and FLRGs are  $\sigma_{v, \text{off}}^{\text{BLRG}} = 519 \pm 48$  km/s and  $\sigma_{v, \text{off}}^{\text{FLRG}} = 561 \pm 37$  km/s for the Lorentzian FoG effect, and  $\sigma_{v, \text{off}}^{\text{BLRG}} = 498 \pm 41$  km/s and  $\sigma_{v, \text{off}}^{\text{FLRG}} = 512 \pm 32$  km/s for the Gaussian FoG effect, respectively. For the Mean center,  $\sigma_{v, \text{off}}^{\text{Mean}} \simeq 291 \pm 20$  km/s and  $\sigma_{v, \text{off}}^{\text{Mean}} \simeq 270 \pm 17$  km/s for the Lorentzian and Gaussian FoG models, respectively. Fig.3 shows that the Gaussian FoG model gives a better fit to the scale dependence of the FoG effect measured from the SDSS LRG catalog than the Lorentzian model. The minimum  $\chi^2$  values inferred are for the best-fit models obtained by jointly fitting the model predictions to the BLRG and FLRG power spectra taking into account the cross-covariance. The  $\chi^2$  has fourteen degrees of freedom: sixteen data points minus two model parameters (two  $\sigma_{v, \text{off}}$  parameters). These results are confirmed by the results using the LRG-galaxy weak lensing and the LRG-photo- $z$  galaxy cross-correlation.

### 3.3 LRG-galaxy weak lensing

As the second observable, we use the cross-correlation of LRG-inferred centers with shapes of background galaxies – the so-called galaxy-galaxy lensing using the LRGs as lenses, which was measured in the same way as in M12. In brief, this measurement uses a catalog of 1.2 background galaxies per arcmin<sup>2</sup> with measured shapes from the re-Gaussianization method (Hirata & Seljak 2003) and photometric redshifts from Zurich Extragalactic Bayesian Redshift Analyzer (ZEBRA, Feldmann et al. 2006); the catalog was described and thorough studies of systematic errors were carried out in several recent papers (M12, and also Reyes et al. 2011; Mandelbaum et al. 2012a; Nakajima et al. 2012).

The lensing measurement is done as follows. We first identify background galaxies around each LRG that have photometric redshift larger than the LRG spectroscopic redshift. The weights are assigned to each LRG-background galaxy pair using optimal weighting according to the error on the source shape measurement via

$$w_{ls} = \frac{1}{\Sigma_{\text{crit}}^2 (\sigma_s^2 + \sigma_{SN}^2)}, \quad (19)$$

where  $\sigma_s^2$  is the shape measurement error due to pixel noise, and  $\sigma_{SN}^2$  is the RMS intrinsic ellipticity (both quantities are per component, rather than total; the latter is fixed to 0.365 in M12).  $\Sigma_{\text{crit}}$  is the critical surface mass density defined by  $\Sigma_{\text{crit}}^{-1}(z_l, z_s) \equiv 4\pi G c^{-2} D_{ls} D_l (1+z_l)^2 / D_s$ , where  $D_l$  and  $D_s$  are the angular diameter distances to lens (LRG) and source and  $D_{ls}$  is the distance between them, and we used the best-fit photo- $z$  of each source to compute  $D_s$ ; this gives rise to a bias in the signals that can be easily corrected using the method from Nakajima et al. (2012). The factor  $(1+z_l)^2$  arises due to our use of comoving coordinates. The factor  $\Sigma_{\text{crit}}^{-2}$  downweights pairs that are close in redshift and therefore are inefficient in weak lensing.

The projected mass density in each radial bin can be computed via a summation over lens-source pairs “ $ls$ ” and random lens-source pairs “ $rs$ ”:

$$\Delta\Sigma(R) = \frac{\sum_{ls} w_{ls} e_t^{(ls)}(R) \Sigma_{\text{crit}}(z_l, z_s)}{2\mathcal{R} \sum_{rs} w_{rs}}, \quad (20)$$

where  $e_t$  is the tangential ellipticity component of source galaxy with respect to the lens position, the factor of  $2\mathcal{R}$  is necessary to convert to tangential shear  $\gamma_t$  due to our definition of ellipticity, and  $R$  is the comoving projected radius from lens, which is estimated from the separation angle between lens (LRG) and source on the sky as  $R = \chi_{\text{LRG}} \theta$ . The division by  $\sum w_{rs}$  is necessary to account for the fact that some of our ‘sources’ are physically associated with the lens, and therefore not lensed by it. Finally, we subtract off a similar signal measured around

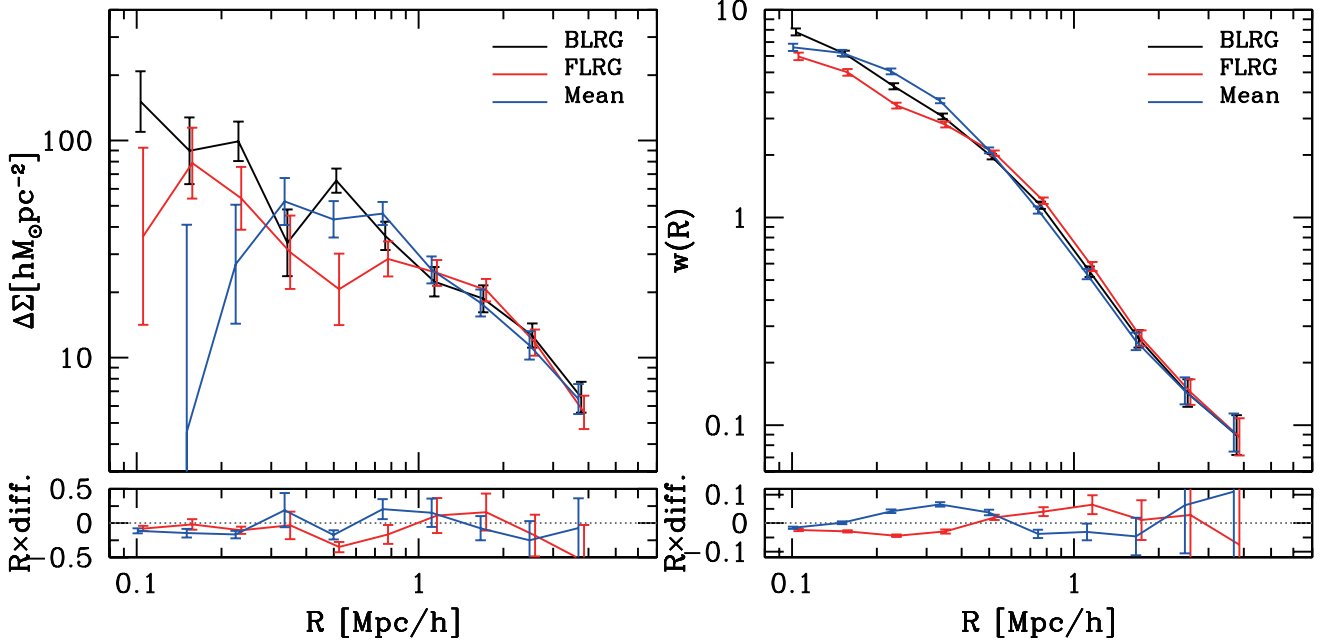


**Figure 4.** *Left panel:* The cross-correlation of LRG-inferred halos with shapes of background, photometric galaxies – the LRG-galaxy weak lensing, measured for the multiple-LRG systems using the BLRG, FLRG or Mean halo center proxies, respectively. The background galaxy sample consists of photometric galaxies with photometric redshifts larger than the LRG redshift (see text for the details). In these lensing measurements, we used the exactly same lens-source pairs and random point catalogs. The three lensing signals at radii  $\gtrsim 1$  Mpc/h are similar, but the signals at smaller radii differ from each other. The lower panel shows the fractional difference of the profile relative to BLRG center, multiplied by  $R$  for illustrative purpose:  $(\text{FLRG}/\text{BLRG}-1) \times R$  or  $(\text{Mean}/\text{BLRG}-1) \times R$ . The error bars for the ratio properly take into account the cross-covariance of the different profiles, because these different-center measurements are from the same multiple-LRG systems as well as from the same population of background galaxies and therefore the errors of the different profiles are highly correlated with each other at each radial bin. *Right panel:* Likewise, the projected cross-correlation function of the LRG-inferred halos with photometric galaxies for the multiple-LRG systems, using the three different centers. The photometric galaxy sample is taken from the photometric galaxies for which the photometric redshift is consistent with the spectroscopic redshift of each LRG halo within the photo- $z$  errors. The measured amplitudes at scales  $R \gtrsim 0.2$  Mpc/h show increasing off-centering effects in the order of the Mean, BLRG and FLRG centers as in the FoG results in Fig.3 (see text for details). The BLRG correlation shows an excess in the power at the small radii,  $R \lesssim 200$  kpc/h. These cross-correlations of different centers can be interpreted by using models with a mixture of centered and off-centered (satellite) LRGs in the host halos (see text for discussion).

random lenses, to subtract off any coherent systematic shear contributions (Mandelbaum et al. 2005); this signal is statistically consistent with zero for all scales used in this work.

To calculate the error bars, we used the jackknife resampling method, as for the power spectrum measurement. The maximum scale used for the fits in the lensing analysis is a few Mpc, within a factor of two of the virial radius of massive halos; this corresponds to several arcminutes at the typical LRG redshift, which is  $< 0.01$  times the typical size of each jackknife resampled region. Thus, the jackknife method is a reasonable approach to getting the covariance matrix for the projected mass profile.

The left panel of Fig.4 shows the LRG-shear cross-correlation measured for the multiple-LRG systems, using the different halo centers (Mean, BLRG and FLRG). We used the same pairs of lens and sources, and therefore the difference in the measured correlations arises from the different centers. We are plotting only the radii relevant for the virial region of massive halos, up to a few Mpc. The three mass profiles agree with each other at radii  $\gtrsim 1$  Mpc/h, reflecting that the three centers are in the same halos. However, the mass profiles differ at smaller radii. The intermediate scales around 0.5 Mpc/h show that the lensing signals for the BLRG and Mean centers are higher than the FLRG signal, consistent with our interpretation of the FoG measurements in Fig.3. At the smaller scales, the mass profile for the Mean center shows a decreasing power with decreasing radii, which is a clear signature of the dilution effect due to the off-centering effect and the lack of a galaxy at that position. On the other hand, the mass profiles of the BLRG and FLRG centers do not show this dilution at the smallest scales.

In Fig.5, we show the results of fitting the halo model prediction from Section 2.3 to the measured lensing profiles for the three centers in the left panel of Fig.4. The fit includes 10 model parameters

$$p_{\alpha} = (\bar{M}_{180b}, \bar{c}_{180b}, q_{\text{cen}}^{\text{BLRG}}, R_{\text{off}}^{\text{BLRG}}, m_{\text{sh}}^{\text{BLRG}}, q_{\text{cen}}^{\text{FLRG}}, R_{\text{off}}^{\text{FLRG}}, m_{\text{sh}}^{\text{FLRG}}, R_{\text{off}}^{\text{Mean}}, \bar{b}), \quad (21)$$

where  $\bar{M}_{180b}$  and  $\bar{c}_{180b}$  are the average mass and concentration parameter of NFW profile for host halos of the multiple-LRG systems,  $q_{\text{cen}}$  is the fraction of the BLRGs or FLRGs that are central galaxies in their host halos,  $R_{\text{off}}$  is the typical off-centering radius (see Eq. 1),  $m_{\text{sh}}$  is the sub-halo mass hosting the BLRG or FLRG, and  $\bar{b}$  is the bias parameter for the 2-halo term of the projected mass profile (Eq. 9). We note that we use the same parameters of the host halo,  $(\bar{M}_{180b}, \bar{c}_{180b})$ , when jointly fitting the model to the measured mass profiles of the three centers, because the three measurements used exactly the same catalog of multiple-LRG systems. We do not assume a fixed value for the halo bias, instead treating  $\bar{b}$  as a free parameter to absorb any uncertainties in the modeling of this term (e.g., linear vs. nonlinear power spectrum,

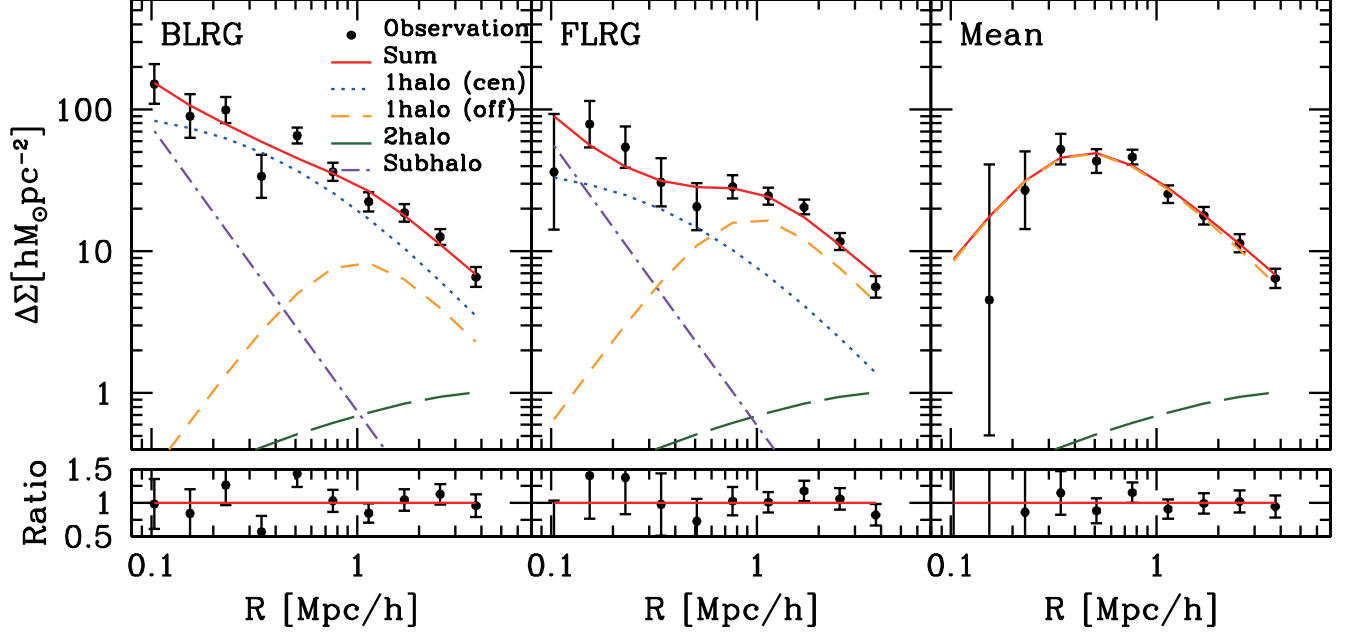


**Figure 5.** The best-fit halo model predictions, developed in Section 2.3, to the measured LRG-galaxy lensing signals, for the BLRG (left panel), FLRG (middle) and Mean (right) centers, respectively. The lower panel in each plot shows the ratio of the best-fit model to the measured profile. The data with error bars are the same as in the left panel of Fig.4. We considered the lensing contributions from the host halos of the multiple-LRG systems and from the sub-halo hosting the BLRG or FLRG at small scales. For the host halo contribution, we considered 3 contributions: the 2-halo term (dashed curve) and the 1-halo terms with and without the off-centering effect, indicated by the long- and short-dashed curves, respectively. For the BLRG- and FLRG-centers, we assumed that some fraction of the BLRGs or FLRGs are central galaxies, modeled by  $q_{\text{cen}}$  (see Eq. 21), while the remaining LRGs are off-centered (satellite) LRGs. On the other hand, we assumed that all the Mean centers have offsets from the true center in each host halo. The dot-dashed curve is the sub-halo lensing contribution for which we assumed a point mass. The top solid curve in each panel is the total lensing signal including all contributing terms. Note that the mass and concentration parameters of the host halos are the same in the three panels, since the same set of halos was used in each case (we simultaneously fit the model to the three measurements).

Best-fit model parameters

Measurement	$q_{\text{cen}}^{\text{BLRG}}$ [per cent]	$R_{\text{off}}^{\text{BLRG}}$ [Mpc/h]	$m_{\text{sh}}^{\text{BLRG}}$ [ $10^{12} M_{\odot}/h$ ]	$q_{\text{cen}}^{\text{FLRG}}$ [per cent]	$R_{\text{off}}^{\text{FLRG}}$ [Mpc/h]	$m_{\text{sh}}^{\text{FLRG}}$ [ $10^{12} M_{\odot}/h$ ]	$R_{\text{off}}^{\text{Mean}}$ [Mpc/h]	$\bar{M}_{180b}$ [ $10^{14} M_{\odot}/h$ ]	$\bar{c}_{180b}$
$\Delta\Sigma(R)$	$63 \pm 21$	$0.44 \pm 0.22$	$2.3 \pm 1.4$	$24 \pm 13$	$0.39 \pm 0.06$	$1.9 \pm 1.1$	$0.16 \pm 0.03$	$1.63 \pm 0.16$	$4.8 \pm 1.4$
$w^{\text{cross}}(R)$	$54 \pm 5$	$0.35 \pm 0.02$	–	$32 \pm 3$	$0.40 \pm 0.01$	–	$0.19 \pm 0.01$	–	–

**Table 2.** The best-fit values and marginalized errors of the model parameters obtained from the fitting of the models to measurement of the LRG-galaxy weak lensing or, separately, the projected cross-correlation of LRGs and photo- $z$  galaxies (Fig.4). We focused on the multiple-LRG systems for the measurements, and the error bar of each parameter is the  $1\text{-}\sigma$  uncertainty including marginalization over other parameters.

linear bias only, etc.). This is acceptable because even at the maximum scales shown on the plot, the 2-halo term is subdominant to the 1-halo term. We assumed a narrow mass range of the host halos. We also assume that all the “Mean centers” in all the multiple-LRG systems are off-centered (i.e.  $q_{\text{cen}}^{\text{Mean}} = 0$ ) and lack a sub-halo lensing contribution, because the Mean center is not associated with the position of any bright galaxy. Notice that we used the average halo mass parameter, defined as the mass enclosed within a sphere of radius  $r_{180b}$  inside of which the mean density is 180 times the mean background mass density  $\bar{\rho}_{m0}$ . We used the Markov Chain Monte Carlo (MCMC) method to explore the marginalized posterior distribution of each model parameter, by taking into account the significant correlations between the observed lensing profiles using different halo centers, and the different radial bins.

Table 2 summarizes the parameter constraints derived from the measured LRG-galaxy weak lensing. First of all, the host halo mass for the multiple-LRG systems is about  $1.6 \times 10^{14} M_{\odot}/h$ , which is significantly more massive than the average halo mass inferred from the LRG-shear lensing using all the LRG systems, about  $4 \times 10^{13} M_{\odot}/h$  (Mandelbaum et al. 2006a) as explicitly studied in Fig.10. Secondly, the central galaxy fraction for the BLRGs is  $q_{\text{cen}}^{\text{BLRG}} \simeq 63$  per cent, and larger than 24 per cent for the FLRGs. The measured mass profiles favor non-zero  $q_{\text{cen}}$  values at the  $2 - 3\sigma$  level, i.e. some contribution from central LRGs is needed to reproduce the measured profiles. We found non-zero values of the off-centering radius for all three different centers (BLRGs, FLRGs and Mean):  $R_{\text{off}} \simeq 350, 400$  and  $190$  kpc/h for the BLRG, FLRG and Mean centers, respectively, although this detection is not very statistically significant for the BLRG center ( $2\sigma$ ).

The different panels of Fig.5 compare the best-fit model predictions with the measured mass profiles for the three different centers. It is

clear that our model reproduces the measurements very well. The mass profile for the Mean center has a clear signature of dilution due to the off-centering effect. This is reasonable, because we do not believe that the Mean position of LRGs happens to coincide with the true center. For the lensing mass profiles for the BLRG and FLRG centers, the best-fit model has two contributions from the central LRGs and from the off-centered (satellite) LRGs. The sub-halo contribution of the BLRG or FLRG is a marginal detection, but implies that the measured lensing profile needs such an additional mass concentration relative to the smooth NFW profile, which can be caused by two effects: the sub-halo hosting the satellite LRGs, or the baryonic concentration effect on the total mass around the central LRGs (Schulz et al. 2010). The sub-halo mass we measured could be due to these effects and therefore is difficult to interpret physically; furthermore, the detection significance is quite low,  $< 2\sigma$  for both BLRG and FLRG.

Since we now have constraints on the mass profile of host halos and the typical off-centering radius for the different halo centers, we can infer the typical velocity dispersion of the off-centered LRGs based on the virial theorem (Hikage et al. 2012):

$$\sigma_{\text{off},v}^2(r) = \frac{GM(< r)}{2r}. \quad (22)$$

The enclosed mass within a sphere of radius  $R_{\text{off}}$  for an NFW halo is given as  $M(< R) = M_{180b} f(c_{180b} R/R_{180b})/f(c_{180b})$ , where  $f(x) \equiv \ln(1+x) - x/(1+x)$  and  $M_{180b}$ ,  $R_{180b}$  and  $c_{180b}$  are the virial mass, virial radius and the halo concentration for the mass definition with respect to 180 times the mean mass density. As can be found from Table 2, if we assume  $M_{180b} = 1.6 \times 10^{14} M_{\odot}/h$ ,  $c_{180b} = 4.8$ , and the offset radii of  $R_{\text{off}} = 440$  and  $390$  kpc/ $h$  for the off-centered BLRGs and FLRGs, the virial theorem above gives  $\sigma_{v,\text{off}} \simeq 516$  and  $511$  km/s, respectively. To be more precise, we estimate the typical velocity dispersion for the off-centered LRGs by weighting the velocity dispersion in the above equation with the off-centering profile with width of  $R_{\text{off}}$  (Eq. 1). These velocity dispersions are consistent with those inferred from the FoG measurements in Fig.3 (which imply  $\sigma_{v,\text{off}} \simeq 500$  km/s).

Finally we comment on the significance of the detection of off-centered BLRGs. As we discussed, the fraction of off-centered BLRGs,  $q_{\text{cen}}^{\text{BLRG}} = 0.63 \pm 0.21$ , is less than a  $3\sigma$  significance, given the limited signal-to-noise ratios of the lensing profiles for the multiple LRG systems (see Section 5 for a further discussion). One might ask whether the measured lensing profiles for the three centers can be fitted by requiring that all BLRGs sit at the true center of each halo, i.e.  $q_{\text{cen}}^{\text{BLRG}} = 1$  and  $R_{\text{off}}^{\text{BLRG}} = 0$ . The best-fit  $\chi^2$  is degraded only by  $\Delta\chi_{\text{min}}^2 = 2$  compared to our fiducial model, and therefore a detection of the off-centered BLRGs is not significant, less than a  $2\sigma$  level. In this case, the best-fit values for other parameters are changed from Table 2;  $\bar{M}_{180b} = 1.63 \rightarrow (1.59 \pm 0.14) \times 10^{14} M_{\odot}/h$ ,  $\bar{c}_{180b} = 4.8 \rightarrow 3.3 \pm 0.5$ ,  $q_{\text{cen}}^{\text{FLRG}} = 0.24 \rightarrow 0.32 \pm 0.15$ ,  $R_{\text{off}}^{\text{FLRG}} = 0.39 \rightarrow (0.37 \pm 0.07)$  Mpc/ $h$ , and  $R_{\text{off}}^{\text{Mean}} = 0.16 \rightarrow (0.12 \pm 0.02)$  Mpc/ $h$ . It is worth noting that the halo concentration derived using the central BLRG assumption,  $\bar{c}_{180b} = 3.3$ , is lower than that predicted for halos of this mass by  $N$ -body simulations. When the lensing results are combined with the cross-correlations of the multiple-LRG halos with the photometric galaxies, which have greater signal-to-noise ratios, we can derive more robust, convincing constraints on the off-center parameters for the BLRGs and FLRGs, as we will show below.

### 3.4 Projected cross-correlation between LRGs and photometric galaxies

As the third observable to constrain the off-centered LRGs, we use the projected cross-correlation function between the LRG-inferred halos and a purely photometric sample of galaxies,  $w^{\text{cross}}(R)$ . The sample used for this calculation was selected in much the same way as the lensing source catalog described in the previous section, but (1) there is no requirement that the galaxy be large enough in angular extent to measure its shape, (2) we impose a brighter flux limit of  $r < 21$  to reduce the effects of photo- $z$  error, and (3) we require that the ZEBRA fit to the galaxy SED be consistent with an early-type galaxy and that the photo- $z$  is consistent with the LRG redshift to within the quoted 68 per cent statistical errors from ZEBRA.

Our measurement of the projected correlation between the LRG-inferred halos ( $H$ ) and fainter photometric red galaxies ( $G$ ) also makes use of a sample of random points ( $R$ ) distributed in the same way as the halos. Given a lower and upper 68 per cent confidence limit on the faint galaxy photo- $z$ ,  $z_{l1}$  and  $z_{u1}$ , we compute the projected correlation via summation:

$$w^{\text{cross}}(R) = \frac{\sum HG(z_{l1} \leq z_H \leq z_{u1})}{\sum RG(z_{l1} \leq z_R \leq z_{u1})} - 1, \quad (23)$$

where the projected radius is estimated from the redshift of the LRG halo and the angular separation between the halo center and the photometric galaxy,  $R = \chi_{\text{LRG}} \Delta\theta$ . The cross-correlation method is very powerful to distinguish the photometric galaxies that are physically associated and therefore clustered with the spectroscopic LRG halos. Including photometric galaxies that are not associated with LRGs, and appear at that redshift due to photo- $z$  error, causes a dilution of the correlation signals. Hence, we will not use the amplitude information for the following parameter estimation. Similarly to the LRG-galaxy lensing measurement, we estimate the covariance matrix of  $w^{\text{cross}}(R)$  via the jackknife resampling method.

The right panel of Fig.4 shows the measured cross-correlation,  $w^{\text{cross}}(R)$ , for the three halo centers. We again note that we worked on the same set of multiple-LRG systems for the three centers, and the difference between the three cross-correlation measurements is only due to the positions of the LRG-inferred halo centers. Interestingly, over the intermediate range of radii,  $R \simeq [0.15, 0.5]$  Mpc/ $h$ , the correlation functions have greater amplitudes in the order of the Mean, BLRG and FLRG centers. Then, for the larger radii,  $R \gtrsim 0.5$  Mpc/ $h$ , the

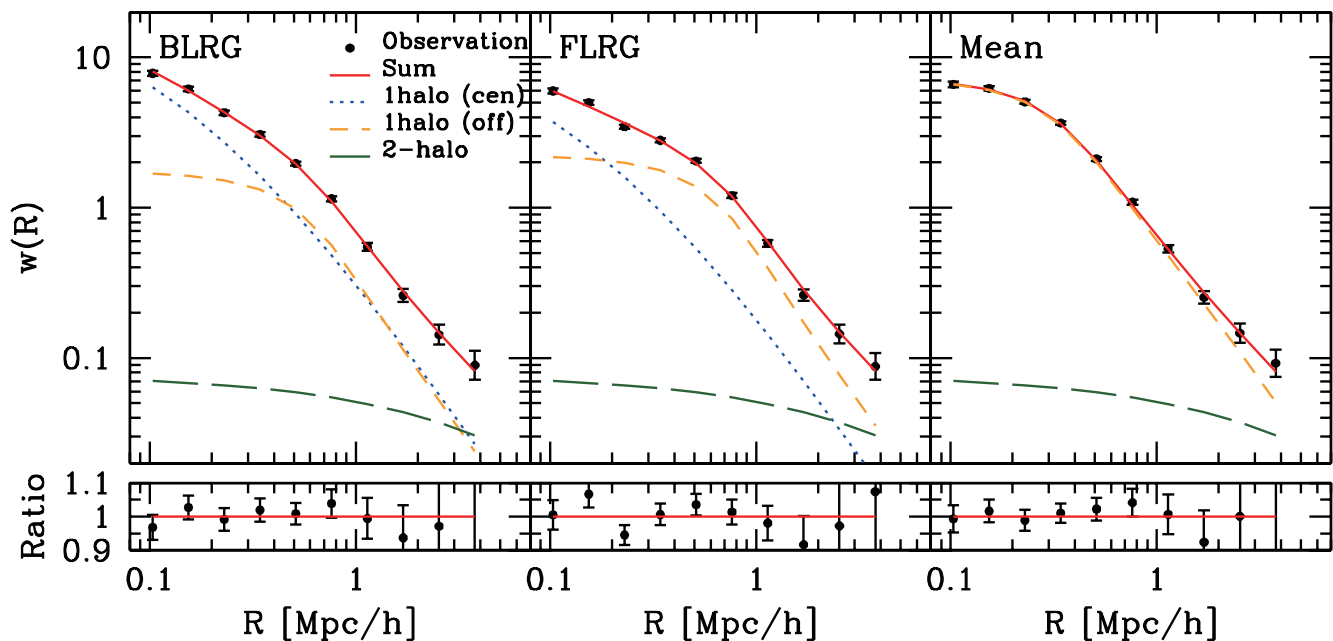


**Figure 6.** The best-fit model predictions obtained by fitting the models (see Section 2.4) to the projected cross-correlation functions of the LRG-inferred halos with the photometric galaxies, for the BLRG (*left panel*), FLRG (*middle*), and Mean (*right*) centers, respectively. As in Fig.5, we assumed that only some fraction of the BLRGs or FLRGs are off-centered galaxies. By using a model containing a mixture of central and satellite LRGs, we can reproduce the measured projected correlation functions over the entire range of radii we consider. The lower plot in each panel shows a remarkably good agreement between the best-fit model and the measured profile for each center.

correlation amplitudes are in the opposite order, greater in the order of the FLRG, BLRG and Mean centers<sup>14</sup>. As can be found from Fig.1, these behaviors are exactly what is expected for the off-centering effects, because the off-centering effect causes a transfer of the power of the correlation function from smaller to larger radii relative to the typical off-centering radius, *regardless* of the underlying true radial distribution of photometric galaxies in the LRG-inferred halos. The order of the off-centering amounts for the BLRG, FLRG and Mean centers is in good agreement with the FoG measurements in Fig.3, and also consistent with the weak lensing measurements in the left panel of Fig.4. The statement that the Mean center is, in a statistical sense, closer to the true center than the BLRG center for the multiple-LRG halos is favored by the relative amplitude differences between the BLRG and Mean centers in the different ranges of radii;  $w^{\text{BLRG}}(R) > w^{\text{Mean}}(R)$  in the range  $0.15 \lesssim R \lesssim 0.5 \text{ Mpc}/h$ ,  $w^{\text{BLRG}}(R) < w^{\text{Mean}}(R)$  in the range  $0.5 \lesssim R \lesssim 2 \text{ Mpc}/h$ , and  $w^{\text{BLRG}}(R) \simeq w^{\text{Mean}}(R)$  at the larger radii as can be found from Fig.1. On the other hand, the correlation function for the BLRG center shows the greatest amplitude at the very small radii,  $R \lesssim 0.15 \text{ Mpc}/h$ , which is not as expected from the off-centering effect. We will show below that the measurements can be nicely explained by including a mixture of central and satellite LRGs in the multiple-LRG systems into the halo model predictions.

Similarly to the LRG-galaxy lensing, we fit the halo model in Section 2.4 to the projected correlation functions. To be more precise, we use the following model parameters:

$$p_\alpha = (\Delta z_{\text{phz}}, \bar{M}_{180b}, \bar{c}_{180b}^g, q_{\text{cen}}^{\text{BLRG}}, R_{\text{off}}^{\text{BLRG}}, q_{\text{cen}}^{\text{FLRG}}, R_{\text{off}}^{\text{FLRG}}, R_{\text{off}}^{\text{Mean}}, \bar{b}^2), \quad (24)$$

where  $c_{180b}^g$  is the effective concentration parameter to model the radial distribution of photometric galaxies by an NFW model. Most of the parameters are the same as those for the LRG-galaxy lensing analysis (Eq. 21), except for the parameter  $\Delta z_{\text{phz}}$  and  $\bar{b}^2$ . We again note that we employ the same parameters of the host halo,  $(\bar{M}_{180b}, \bar{c}_{180b})$ , when jointly fitting the model to the three cross-correlation functions for BLRG, FLRG and Mean centers, because the three measurements used exactly the same catalog of multiple-LRG systems and photometric galaxies. The parameter  $\Delta z_{\text{phz}}$  is a nuisance parameter to model the dilution factor,  $\bar{n}_{\text{phg}}^{2\text{D}}(z_{\text{LRG}})/\bar{n}_{\text{phg,all}}^{2\text{D}}$ , that arises from a contamination of unassociated photometric galaxies due to photo- $z$  errors as we discussed above. We also include the bias parameter  $\bar{b}^2$  to account for an uncertainty in the 2-halo term amplitude (which is for  $\bar{b}_{\text{LRG}}\bar{b}_{\text{phg}}$  in Eq. 14). In our fitting, we assumed a single (i.e. very narrow) mass bin for host halos of the multiple-LRG systems, and that the distribution of photometric galaxies in the halos follows an NFW profile (see below for the results obtained by relaxing the NFW assumption).

Table 2 shows the best-fit value and the marginalized  $1\sigma$  errors for each parameter. The results are in remarkably good agreement with the LRG-galaxy lensing results within the error bars, while the two measurements are independent in a sense that they are subject to largely

<sup>14</sup> While the magnitude of this effect appears small within the errors on the curves, the signals are highly correlated such that the statistical significance of these orderings is high as can be found from the lower panel of Fig.4.

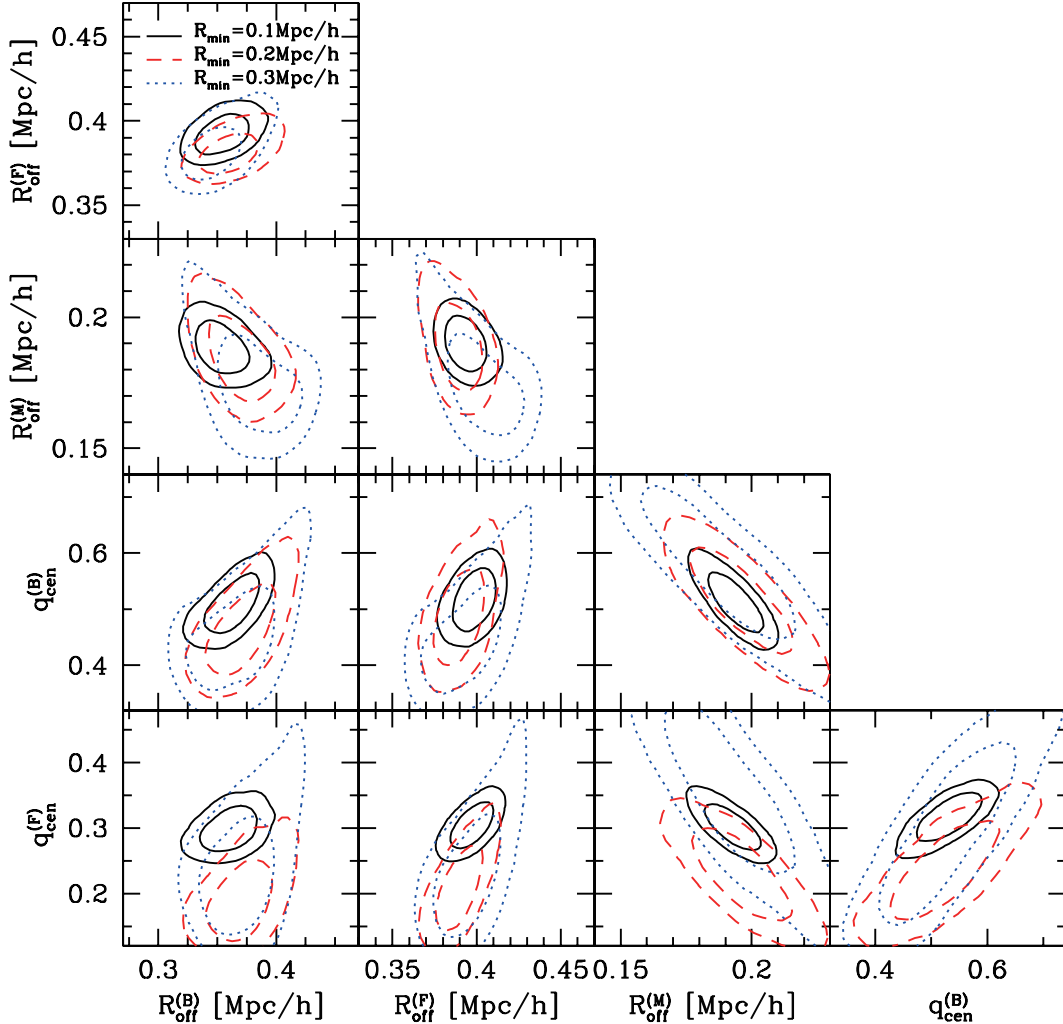


**Figure 7.** The marginalized constraint contours (68 and 95 per cent C.L.) in two-dimensional sub-spaces of the off-centering parameters. The dotted, dashed and solid contours in each panel show the results when we change the minimum radius for the fit to the cross-correlation functions of LRGs and photometric galaxies in Fig.6,  $R_{\min} = 0.3, 0.2$  and  $0.1$  Mpc/h. Including the smaller-radius cross-correlation helps to break the parameter degeneracies, especially the fraction of central LRGs,  $q_{\text{cen}}$ .

different systematic errors, and used different catalogs of photometric galaxies: the background galaxies behind the LRGs and the galaxies at the same redshift as the LRGs, respectively.

Fig.6 shows the best-fit model predictions compared with the measurements. The halo model can well reproduce the measured correlation functions over all the range of radii we consider, including the enhancement in the correlation amplitude at the small radii for the BLRG center. Even for the small error bars, our best-fit model gives a surprisingly good fit to the three cross-correlation functions simultaneously, as explicitly shown in the lower panels for each center.

In Fig.7, we show the marginalized constraint contours in each two-dimensional sub-space of the off-centering parameters. Comparing the dotted, dashed and solid contours shows how the parameter degeneracies are broken by changing the smallest radius down to which the cross-correlation signals are included in the model fitting. It is clear that the enhancement in the cross-correlation amplitudes at small radius,  $R \lesssim 0.3$  Mpc/h, helps to break parameter degeneracies, especially to constrain the central galaxy fraction parameters  $q_{\text{cen}}$ .

Fig.8 compares the constraint contours obtained from the model fitting to the LRG-galaxy weak lensing and the LRG-photometric galaxy cross-correlations. The figure shows that the two results are in good agreement with each other within the errors, and that the cross-correlation gives tighter constraints on the off-center parameters than the weak lensing due to the higher signal-to-noise ratios. The difference in  $S/N$  between the two types of measurements will likely be different in deeper upcoming lensing surveys than it is in SDSS.

One uncertainty in our halo model is the assumption that the radial distribution of photometric galaxies follows an NFW profile. This does not necessarily hold for the SDSS galaxies. In Appendix A, we study how the best-fit off-center parameters are changed if we relax the NFW assumption. In doing so, we used a generalized radial profile given by  $n_g(r) \propto 1/[r^\alpha(1+r/r_s)^{\beta-\alpha}]$  and allow the additional profile parameters  $(\alpha, \beta)$  to freely vary in the model fitting, in addition to  $(\bar{M}_{180b}, \bar{c}_{180b}^g)$  (hence, 2 additional free parameters). As shown in detail in Appendix A, we found that the best-fit off-center parameters and their uncertainties are almost unchanged. To be more explicit, the



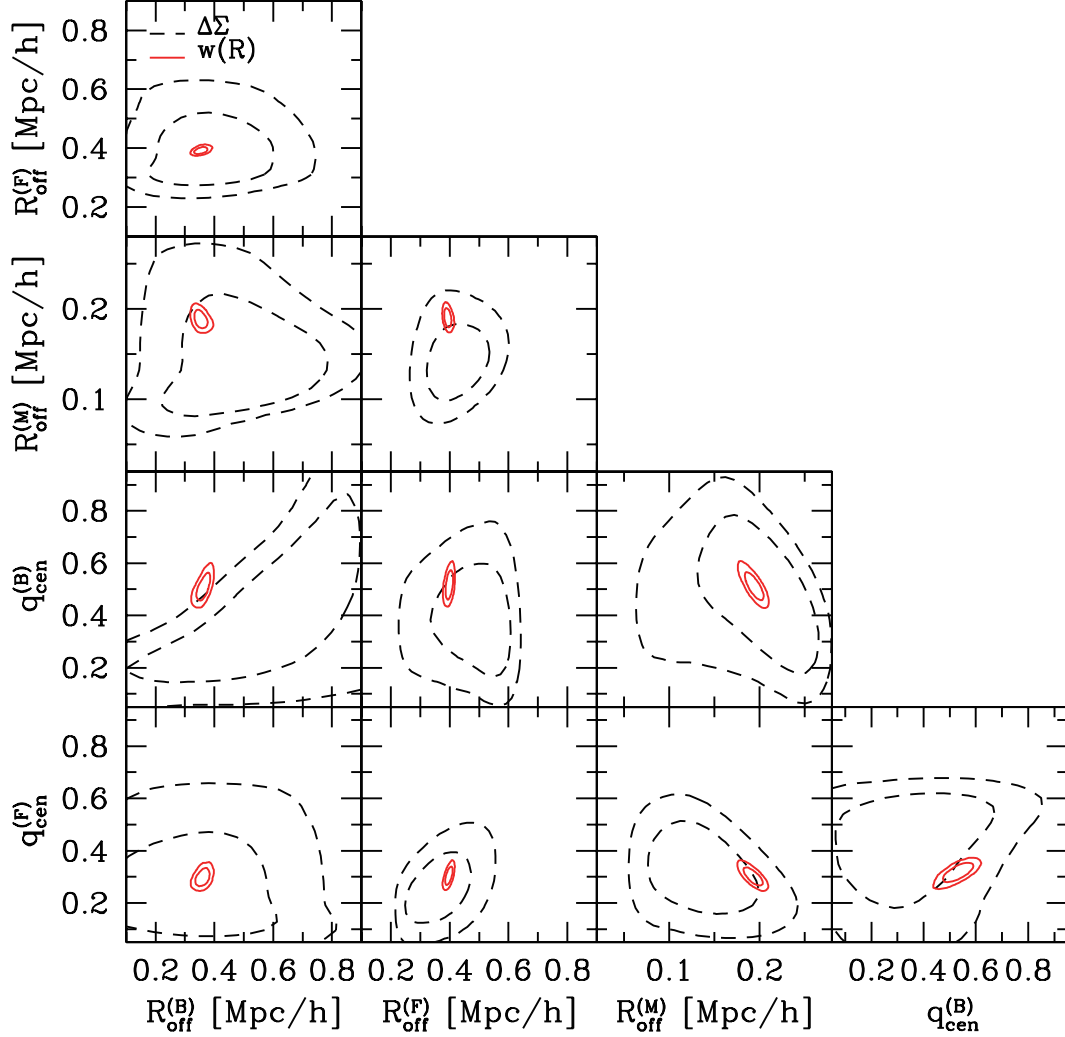


**Figure 8.** Similar to the previous figure, but comparing the 68 and 95 per cent C.L. marginalized constraint contours obtained from the LRG-galaxy weak lensing measurements (dashed contours) and the LRG-photometric galaxy cross-correlation (solid).

best-fit parameters are  $q_{\text{cen}}^{\text{BLRG}} = 0.53 \pm 0.05$ ,  $R_{\text{off}}^{\text{BLRG}} = (0.34 \pm 0.02) \text{ Mpc}/h$ ,  $q_{\text{cen}}^{\text{FLRG}} = 0.32 \pm 0.03$ ,  $R_{\text{off}}^{\text{FLRG}} = (0.39 \pm 0.01) \text{ Mpc}/h$ , and  $R_{\text{off}}^{\text{Mean}} = (0.019 \pm 0.01) \text{ Mpc}/h$ , which are compared with the values in Table 2. Thus we conclude that the off-center parameters derived by our method are relatively insensitive to the profile parameters, because the constraints are derived by comparing the different cross-correlation functions for different centers using the *same* halo and photometric galaxy catalogs, as well as by including marginalization over the profile parameters. We also stress that our results suggest that the radial distribution of photometric member galaxies in cluster-scale halos of  $\sim 10^{14} M_{\odot}/h$  is reasonably well described by a generalized NFW profile with free concentration parameter (also see Berlind & Weinberg 2002; More et al. 2009; Chen 2009; Guo et al. 2012). However, we have not quantitatively explored the impact of more free models, so the specific constraints that we quote for  $q_{\text{cen}}$  and  $R_{\text{off}}$  do contain some assumption regarding the profile of photometric galaxies. Since other studies have not suggested that these distributions are, on average, pathological enough that they cannot be described by a generalized NFW with free concentration, this assumption is not in practice a significant weakness in our results.

As for the lensing profiles in Section 3.3, one might wonder whether the measured cross-correlation functions can be interpreted by imposing all the BLRGs to be at the true center in each halo,  $q_{\text{cen}}^{\text{BLRG}} = 1$  and  $R_{\text{off}}^{\text{BLRG}} = 0$ . If we employ this hypothesis, we can realize that the BLRG cross-correlation,  $w^{\text{BLRG}}(R)$ , gives the average radial distribution of photometric galaxies in the multiple-LRG halos, while the FLRG profile,  $w^{\text{FLRG}}(R)$ , arises from a convolution of the radial distribution of photometric galaxies with the radial distribution of FLRGs in the same host halos. Since our halo model assuming a generalized NFW profile ( $n_g(r) \propto 1/[r^{\alpha}(1+r/r_s)^{\beta-\alpha}]$ ) gives a good fit to the measured profiles, we can use the 1-halo term profiles to infer the radial profiles of the photometric galaxies and FLRGs:

$$\begin{aligned} \tilde{u}_g(k) &= q_{\text{cen}}^{\text{BLRG}} \tilde{u}_{\text{gNFW}}(k) + (1 - q_{\text{cen}}^{\text{BLRG}}) \tilde{p}_{\text{off}}^{\text{BLRG}}(k; R_{\text{off}}^{\text{BLRG}}) \tilde{u}_{\text{gNFW}}(k), \\ \tilde{u}_g(k) \tilde{P}_{\text{off}}^{\text{FLRG}}(k) &= q_{\text{cen}}^{\text{FLRG}} \tilde{u}_{\text{gNFW}}(k) + (1 - q_{\text{cen}}^{\text{FLRG}}) \tilde{p}_{\text{off}}^{\text{FLRG}}(k; R_{\text{off}}^{\text{FLRG}}). \end{aligned} \quad (25)$$

The terms on the r.h.s. of the above equations are our models allowing the off-centered BLRGs:  $q_{\text{cen}}^{\text{BLRG}}$  or  $q_{\text{cen}}^{\text{FLRG}}$  is the fraction of central

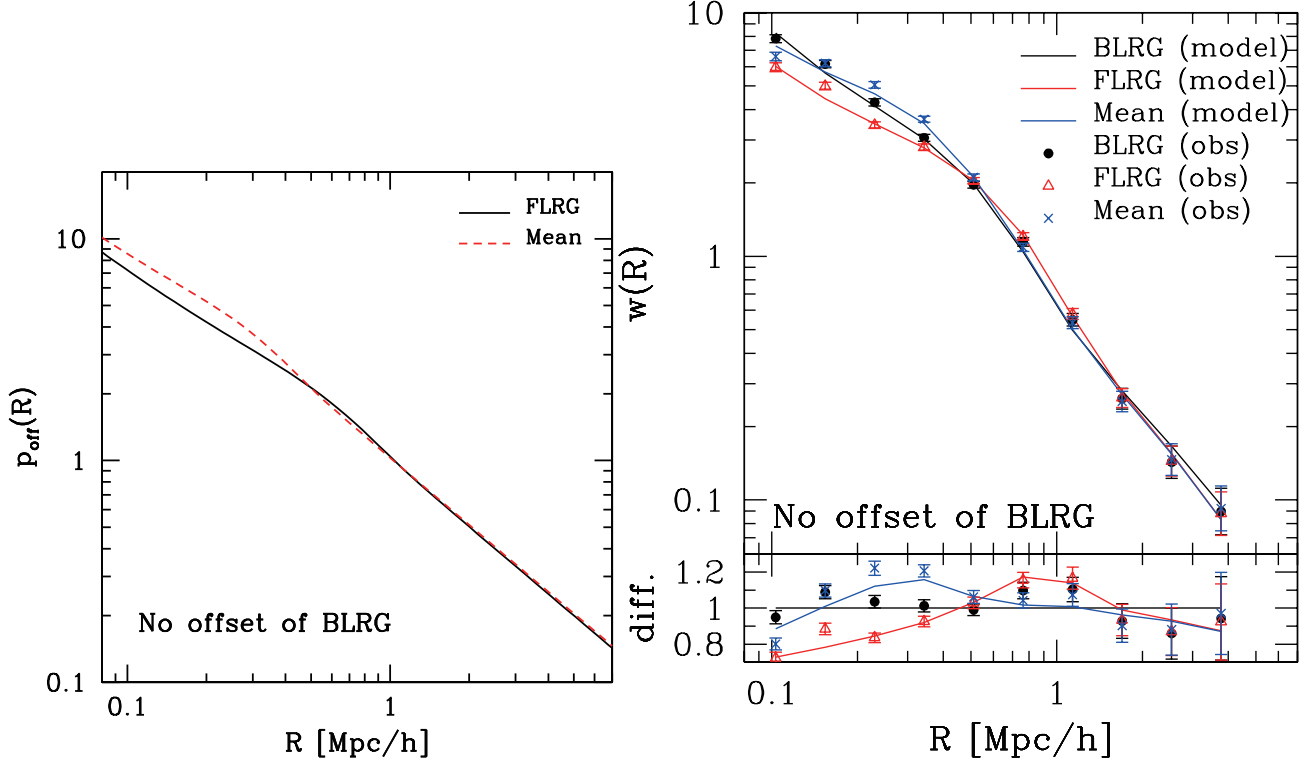


**Figure 9.** A test of the central BLRG hypothesis for an interpretation of the cross-correlation measurements in Fig. 6, i.e. all the BLRGs are at the true center in each of the multiple-LRG system halos. Assuming that all the multiple-LRG systems are systems having 2 LRGs inside and therefore the Mean position in each host halo has a half of the off-center radius of FLRG, the radial (off-center) distribution of FLRG or Mean center proxy can be estimated by using the halo model with a generalized NFW profile to model the radial distribution of member galaxies (see text around Eq. 25 and Appendix A for details). To include uncertainties in the model parameters allowed by the measurement errors, we obtained the best-fit model by varying the model parameters. The  $\chi^2$  value for the best-fit model,  $\chi^2_{\min} = 84$ , can be compared to  $\chi^2_{\min} = 21$  for the best-fit model allowing  $q_{\text{cen}}^{\text{BLRG}} \neq 1$ ; therefore  $\Delta\chi^2 = 63$ , about  $8\sigma$  deviation. *Left panel:* The normalized radial profiles of FLRG and Mean center proxies for the best-fit model with  $q_{\text{cen}}^{\text{BLRG}} = 1$ . *Right panel:* The best-fit model profiles for BLRG, FLRG and Mean center proxies compared with the data (where the data points are the same as in the right panel of Fig. 4). The lower panel shows the fractional difference of the best-fit model or the measured profile relative to the best-fit model profile for BLRG. The model profiles show sizable differences from the measured profile for each of the three centers over the different range of radii.

BLRGs or FLRGs,  $\tilde{p}_{\text{off}}^{\text{BLRG}}$  or  $\tilde{p}_{\text{off}}^{\text{FLRG}}$  is the Fourier transform of the radial distribution of off-centered FLRGs or BLRGs, and  $\tilde{u}_{\text{gNFW}}(k)$  is the Fourier transform of the generalized NFW profile to model the radial distribution of member galaxies, which is given by 4 free parameters ( $M_{180b}, c_{180b}^g, \alpha, \beta$ ) (see Appendix A for details). The terms on the l.h.s are from the central BLRG hypothesis:  $\tilde{u}_g(k)$  is the Fourier transform of the radial distribution of photometric galaxies, and  $\tilde{P}_{\text{off}}^{\text{FLRG}}(k)$  is the Fourier transform of the radial distribution of FLRGs. In this way, we can derive  $\tilde{u}_g(k)$  and  $\tilde{P}_{\text{off}}^{\text{FLRG}}(k)$  in Fourier space. Then, assuming that all the multiple-LRG systems are systems with 2 LRGs inside, which is a good approximation as found from Table 1, the radial profile of the Mean centers can be simply obtained as  $\tilde{P}_{\text{off}}^{\text{Mean}}(k) \simeq \tilde{P}_{\text{off}}^{\text{FLRG}}(2k)$ , where “2” in the argument arises because we stretch the FLRG profile by a factor of 2 in Fourier space to obtain the Mean profile (shrink the radial profile by a factor of 2 in real space). Thus, by inverse Fourier-transforming the product  $\tilde{u}_g(k)\tilde{P}_{\text{off}}^{\text{Mean}}(k)$ , we can obtain the radial profile for Mean centers predicted from the central BLRG hypothesis. To include the effect of possible variations in the model parameters within the measurement errors, we searched the best-fit model by varying the model parameters (the parameters on the r.h.s. of Eq. 25). Fig. 9 shows the best-fit model predictions for the radial profiles of FLRG and Mean center proxies and the cross-correlation profiles for BLRG, FLRG and Mean center proxies, respectively. The minimum  $\chi^2$  value for the best-fit model,  $\chi^2_{\min} = 84$ , should be compared to  $\chi^2_{\min} = 21$  for the best-fit model that allows  $q_{\text{cen}}^{\text{BLRG}} \neq 1$ . Compared to the lower panels in Fig. 6, the model profiles show sizable differences from the measured profiles for each of the BLRG, FLRG and Mean center proxies. Although the reconstruction method relies on the assumption that the radial profiles for the photometric galaxies and FLRGs are described by our adopted functional forms (generalized NFW for the former and Gaussian profile for the latter) even outside the range of radii in the measurements, the results again disfavor the central BLRG hypothesis.

#### 4 IMPLICATION FOR THE RESIDUAL FOG EFFECT IN THE LRG POWER SPECTRUM

We have so far shown that three different measurements (the angle-averaged redshift-space power spectrum, the LRG-shear correlation function and the cross-correlation of LRGs and photometric galaxies), all imply the existence of satellite (off-centered) LRGs for the multiple-

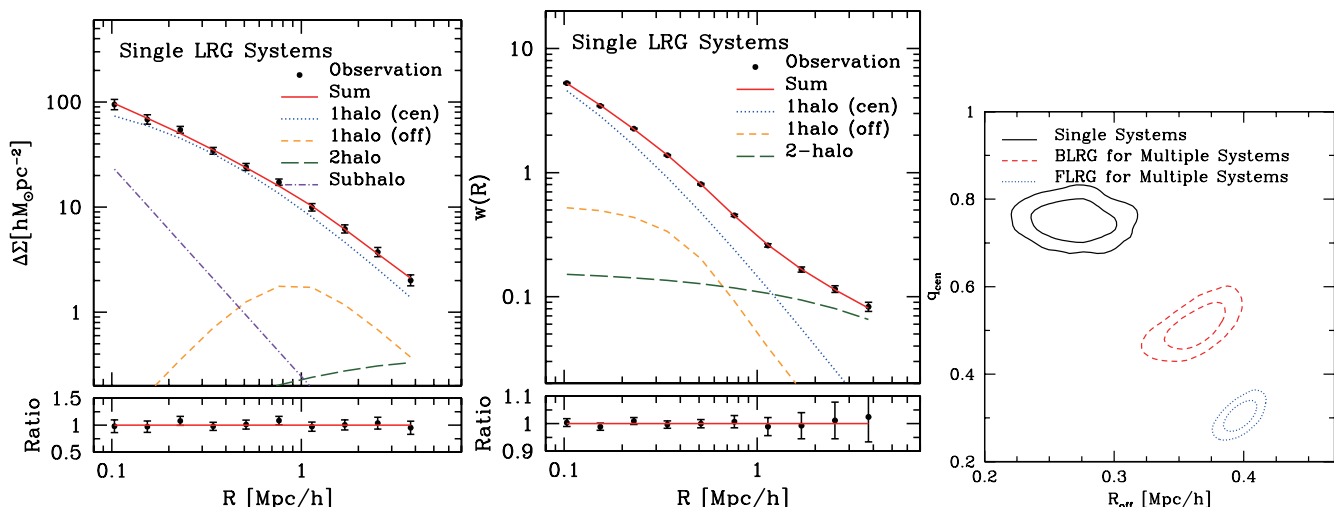


**Figure 10.** The measured LRG-galaxy weak lensing (*Left panel*) and the cross-correlation of LRGs with photometric galaxies (*Middle*) for the single LRG systems. In each panel, the different curves show the best-fit halo model predictions including the contributions from the centered and off-centered LRGs, as in Figs. 5 and 6. However, in the model fitting we employ several simplified assumptions for the fitting for simplicity: we assume a narrow mass bin for the host halo and a thin redshift bin for the single LRG systems, and assume that the dark matter and the photometric galaxies in the host halos follow an NFW profile. The LRG-galaxy lensing gives  $M_{180b} \simeq (0.42 \pm 0.04) \times 10^{14} M_{\odot}/h$  for the best-fit average mass for the host halos, which is smaller than that for the multiple-LRG systems,  $M_{180b} \simeq 1.6 \times 10^{14} M_{\odot}/h$  (see Table 2). *Right panel:* the best-fit off-centering parameters obtained from the cross-correlation measurement are  $q_{cen} = 0.76 \pm 0.06$  and  $R_{off} = (0.26 \pm 0.03)$  Mpc/h for the fraction of central LRGs and the typical off-center radius, respectively. A non-zero off-centering effect is detected at  $> 2\sigma$  significance, and the amount is smaller than in the multiple-LRG systems. Note that the best-fit parameters for the LRG-galaxy lensing are consistent with the cross-correlation results within the error bars, but have larger error bars.

LRG systems, which represent  $\sim 5$  per cent of the halos hosting LRGs. Perhaps most surprising is that some of BLRGs in the multiple-LRG systems exhibit this off-centering effect. In this section, based on these results, we discuss the implications for possible residual FoG contamination of the LRG power spectrum. For some of the multiple-LRG systems, the BLRG is brighter than the FLRG only by a few tenths of a magnitude (see Fig.2). One might think that the off-centered BLRGs are mainly from the multiple-LRG systems where the BLRG and FLRG have a small magnitude difference and therefore the two LRGs are not different (the FLRGs are central instead). In Appendix B, by dividing the multiple-LRG systems into halved samples which have the larger and smaller magnitude difference between the BLRG and FLRG than the median, we study whether or not the amount of the off-centered BLRGs differs in between the halved samples. We do not find any significant difference for the off-centered BLRGs in the two samples, although the FLRG center shows a significant difference. Therefore, the current data show some off-centering effects for BLRGs in the multiple-LRG systems, irrespective of the magnitude difference between the BLRG and FLRG.

The single-LRG systems, each of which contain only one LRG (see Table 1), constitute about 95 percent of the LRG-inferred halos. Although the LRG in single-LRG systems might have the off-centering effect, we do not have any other proxy of halo center besides the LRG position, unlike in the multiple-LRG systems. Nevertheless, we can estimate the amount of possible off-centering effect as follows.

Fig.10 shows the measured LRG-galaxy lensing and the measured cross-correlation of LRGs with photometric galaxies for the single-LRG systems. As in Figs. 5 and 6, we compare the halo model with the measured correlations, and show the best-fit halo model predictions including contribution of the off-centered LRGs. In this model fitting, we employ several simplified assumptions; we assumed a narrow mass bin for the host halos as well as a thin redshift bin of LRGs, and assumed that the dark matter and the photometric galaxies in the single-LRG systems both follow an NFW profile. The LRG-galaxy lensing gives  $M_{180b} \simeq (0.42 \pm 0.04) \times 10^{14} M_{\odot}/h$  for the best-fit host halo mass, which is less massive than the host halo mass of  $M_{180b} \simeq 1.6 \times 10^{14} M_{\odot}/h$  for the multiple-LRG systems. The cross-correlation gives non-zero off-centering parameters:  $q_{cen} = 0.76 \pm 0.06$  and  $R_{off} = (0.26 \pm 0.03)$  Mpc/h. The LRG-galaxy lensing gives consistent results, but with larger error bars due to the smaller signal-to-noise ratio. However, the constraints on the off-centering parameters are not as robust as those for the multiple-LRG systems, because we cannot compare the measurements for the different halo center proxies and the offsetting parameters are more degenerate with the NFW profile parameters. If we use a generalized profile,  $\rho(r) \propto 1/[r^{\alpha}(1+r/r_s)^{\beta-\alpha}]$ , and allow the two additional parameters ( $\alpha, \beta$ ) to vary, the constraints on the off-center parameters are relaxed to  $q_{cen} = 0.79 \pm 0.08$  and  $R_{off} = 0.26 \pm 0.15$  Mpc/h. The non-zero off-center radius becomes less significant, less than  $2\sigma$  level. Nevertheless, as shown in the lower panel, the best-fit model can well reproduce the measured correlation functions, within the small error bars over the range of radii we consider. The LRG-galaxy lensing profile does not give as tight constraints on the off-center parameters as the cross-correlation, due to the smaller signal-to-noise ratios. Assuming an NFW profile, we obtained  $q_{cen} = 0.76 \pm 0.18$  and  $R_{off} = 0.38 \pm 0.25$  Mpc/h, which is consistent with the constraints from the cross-correlation (also see Appendix C). We again note that the results in Fig.10 suggest that the radial distribution of member galaxies in group-scale halos of  $\sim 4 \times 10^{13} M_{\odot}/h$  is fairly well fitted by a generalized NFW profile with free concentration.

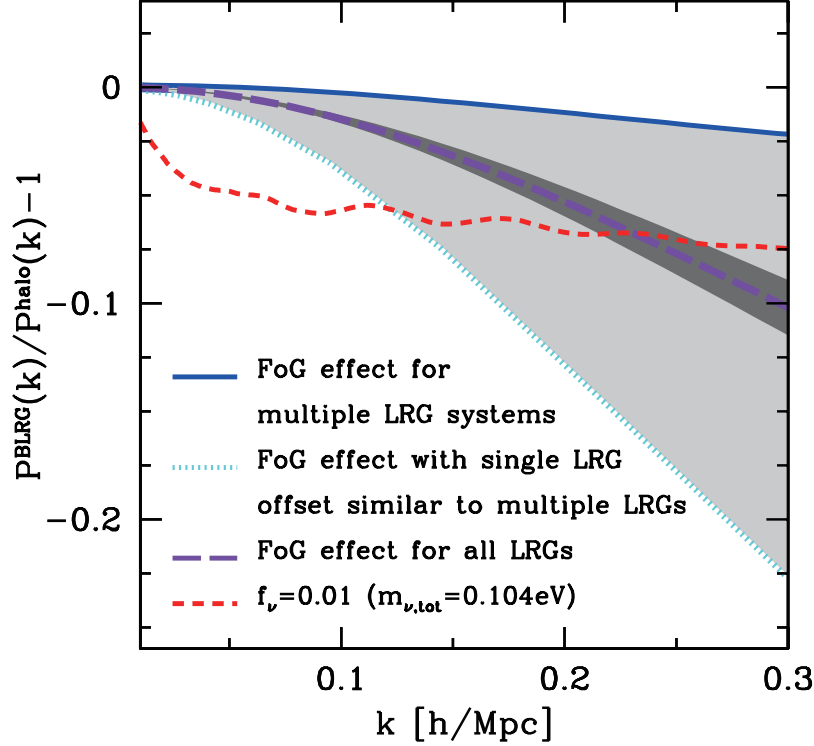


**Figure 11.** Expected FoG suppression of the angle-averaged, redshift-space power spectrum of LRGs using the BLRG center proxy. Here, we show a possible range of the residual FoG contamination relative to the underlying halo power spectrum. The upper solid curve of the shade region shows the FoG effect assuming that only BLRGs in the multiple-LRG systems have the off-centering effects, as in Fig.3. The lower dotted curve shows the FoG effect assuming that BLRGs in the single LRG systems also have off-centering effects, computed based on the halo model in Hikage et al. (2012). For this case, we assumed that the off-centering radius scales with the virial radius of host halos as  $R_{\text{off}} \propto r_{180b}(M)$ , and the FoG amplitude is normalized so as to reproduce the FoG effect at the host halo mass of the multiple LRG systems,  $M_{180b} = 1.67 \times 10^{14} M_{\odot}/h$ . For the fraction of central BLRGs in each halo, we assumed that it varies with host halo mass as  $q_{\text{cen}}^{\text{BLRG}} = 0.6 + 0.05 \ln(M/M_{180b,\text{WL}})$ , and normalized to  $q_{\text{cen}} = 0.6$  at  $M_{180b} = 1.6 \times 10^{14} M_{\odot}/h$ . Thus the dotted curve gives the worst case scenario for the residual FoG effect (see text for details). The bold dashed curve is the FoG effect implied from the constraints on off-centering parameters for the single-LRG systems shown in Fig.10, and the dark shaded region around the curve implies the range covered by  $1\sigma$  uncertainties of the off-centering parameters. For comparison, the dashed curve shows the suppression effect caused by massive neutrinos with total mass  $f_{\nu} = 0.01$  ( $m_{\nu,\text{tot}} = 0.125$  eV). This reveals that the possible FoG effect suggested by the results in this paper can be a serious source of systematic errors in estimating cosmological parameters using the LRG power spectrum without directly modeling the effect.

In Fig.11, we estimate the possible residual FoG contamination in the LRG power spectrum. Shown here is the angle-averaged redshift-space power spectrum for the BLRG center relative to the underlying true halo power spectrum, where we have assumed the linear Kaiser redshift-space distortion effect. Here the shade region shows the allowed range of the residual FoG effect according to the measurements shown in this paper. The upper solid curve is the FoG effect if only BLRGs in the multiple-LRG systems (and not any of the single-LRG systems) have the off-centering effects, i.e. the FoG effect, as we found in Fig.3<sup>15</sup>. Hence, this is a lower limit on the residual FoG effect that should exist in the BLRG power spectrum. The lower dotted curve is the worst-case scenario, which shows the FoG contamination if BLRGs in the single-LRG systems also have the off-centering effects in the host halos. To compute this curve, we used the method developed in Hikage et al. (2012). To be more precise, we assumed that the off-centering radius  $R_{\text{off}}(M)$  scales with the virial radius of host halos as  $R_{\text{off}}(M) \propto r_{180b}(M)$ , and determined the proportional coefficient so that it reproduces the measurement results for the host halo mass of multiple-LRG systems,  $M_{180b} \simeq 1.6 \times 10^{14} M_{\odot}/h$ . In addition, we assumed that the fraction of central BLRGs scales with the halos mass as  $q_{\text{cen}}^{\text{BLRG}} = 0.6 + 0.05 \ln(M/M_{180b,\text{WL}})$ , where the normalization is determined so as to give  $q_{\text{cen}}^{\text{BLRG}} = 0.6$  at  $M_{180b,\text{WL}} = 1.6 \times 10^{14} M_{\odot}/h$ , and the slope 0.05 is taken from the mock galaxy catalog used in Johnston et al. (2007). The genuine FoG effect in the BLRG power spectrum would be inside the shaded region. The thick-dashed curve shows the FoG effect implied from the correlation measurements of the single-LRG systems in Fig.10. The dark shaded region around that curve denotes the range covered by varying the off-centering parameters within the  $1\sigma$  errors. This result might be closer to the genuine effect. However, since the off-centering constraints for the single-LRG systems are

<sup>15</sup> One might notice that the amplitude of the FoG suppression in Fig.11 differs from that in Fig.3. This is because we show the fractional difference of the BLRG power spectrum relative to the spectra for the Mean center or the halo center in Figs. 3 and 11, respectively. Since the power spectrum for the Mean-center also has the FoG suppression as we have shown, the FoG effect for the BLRG spectrum appears to be larger, when plotted with respect to the spectrum for the halo center in Fig.11 than to the spectrum for the Mean center in Figure3.

derived by employing several additional assumptions as we mentioned above, we believe that the entire range within the shaded gray region is still allowed.

Thus, Fig.11 implies that the possible FoG effect can be a systematic error in estimating cosmological parameters if the residual FoG effect is ignored in the model fitting. For example, we show the effect of massive neutrinos on the halo power spectrum as the dashed curve (assuming that the sum of neutrino masses is 0.125 eV, close to the lower bound of the inverted mass hierarchy), but fixing other cosmological parameters to the fiducial values. Since the massive neutrinos cause a suppression in the measured power spectrum, as does the FoG effect, the figure implies that neglecting the FoG effect might cause a serious systematic error in the derived neutrino mass, with the severity of the issue depending on what scales are used.

## 5 DISCUSSION AND CONCLUSIONS

In this paper, we combined three observables (the redshift-space LRG power spectrum, LRG-galaxy weak lensing, and the projected cross-correlation of LRGs and photometric galaxies) to constrain the fraction of satellite LRGs and the average off-centered distribution of the satellite LRGs in the host halos. When doing so, we focused on multiple-LRG systems, about 4000 systems in total (4.5 per cent of all LRG-inferred halos, see Table 1), and compared the measurements obtained by using the different halo center proxies: the positions of the brightest LRG (BLRG), the faintest LRG (FLRG), and the mean positions (Mean) in each multiple-LRG system (Figs. 3 and 4). All three observables consistently imply that some fraction of LRGs are satellites – even those that are the brightest in the halo – and have offsets from the true center. Among the three measurements, the projected cross-correlations of the LRG-inferred halo centers with photometric galaxies show the strongest evidence for off-centered LRGs, even when allowing the satellite galaxies to follow a generalized NFW profile with four free parameters. Perhaps most intriguing or surprising is that some of the BLRGs are satellites and have offsets from the halo center, and the Mean positions tend to be closer to the true center, showing the smallest off-centering effect.

By comparing the halo model developed in Section 2 with the measurements, we constrained the model parameters including the fraction of satellite LRGs and the average off-centering radius (Table 2, and Figs. 3, 5 and 6). A brief summary of our findings is as follows. About 60 and 30 per cent of the BLRGs and FLRGs, respectively, are central galaxies in the host halos of the multiple-LRG systems, and the remaining LRGs are satellite LRGs. If we do not employ a mixture of central and satellite LRGs, we cannot self-consistently model the measurements using different choices for the halo centers. The typical off-centering radius is about 400 kpc/h for both the satellite BLRGs and FLRGs. We also confirmed that the Mean centers just *happen to* be statistically closer to the true center than the BLRG- and FLRG-preferred centers. The LRG-galaxy weak lensing for the Mean centers shows a clear dilution effect on small scales. A similar off-centering radius for the satellite BLRGs and FLRGs might be reasonable, because the FLRGs and BLRGs are both luminous, early-type galaxies, and therefore should have a similar age and history of dynamical friction in the host halos; moreover, the luminosity gap is typically small. The only difference in the off-centering effects arises from the different fractions of central LRGs among the BLRG and FLRGs. Even if using a generalized NFW profile with free concentration, inner and outer slope parameters to model the radial distribution of photometric galaxies, the significance of our detection of satellite BLRGs is not largely degraded. Our results also suggest that the radial distribution of photometric galaxies in cluster- and group-scale halos is fairly well fitted by a generalized NFW profile with free concentration, though the exact values we find (and their errors) are dependent on this assumed distribution for the radial distribution of photometric galaxies.

In these constraints, weak lensing plays a very complementary and unique role, although the signal-to-noise ratio is low due to the small number density of background galaxies in the shallow SDSS catalog. The mean mass of the host halos of the multiple-LRG systems is constrained to be about  $1.6 \times 10^{14} M_{180b}/h$  (with a roughly 10 per cent statistical error); this is indeed more massive than the mean halo mass of all the LRGs. Such large offsets of bright galaxies in massive halos was also suggested recently by Sehgal et al. (2012), based on a study of the stacked Sunyaev-Zel'dovich (SZ) effect via a cross-correlation of the SDSS optically-inferred clusters with the CMB map of the Atacama Cosmology Telescope survey. They noted that one explanation for the unexpectedly smaller SZ signal is large off-centering effects. It would be worth exploring whether our results can resolve the stacked SZ result.

Based on these constraints, we explored the off-centering effects on the underlying redshift-space power spectrum of LRG-inferred halos, and showed the allowed range for the residual FoG contamination in the LRG power spectrum (Fig.11). As the most optimal case, the residual FoG effect is only from the multiple-LRG systems, as we have studied in this paper. As the worst case scenario, by assuming that a majority of LRGs in the (far more numerous) single-LRG systems have similar off-centering effects as in the multiple-LRG systems, we estimated the possible maximum, residual FoG effect on the LRG-inferred power spectrum, based on the method in our earlier paper (Hikage et al. 2012). The genuine amount of residual FoG effect should be between the two cases we show. In particular, the residual FoG effect, if not accounted for, may cause a potentially significant bias in cosmological parameters derived from the measured power spectrum amplitude, e.g. the sum of neutrino masses which likewise causes a suppression in the power spectrum amplitude at small scales. Our results in Fig.11 imply that the bias may not be that significant if using the power spectrum amplitude only up to  $k_{\max} \simeq 0.1 h/\text{Mpc}$ , but may be quite significant if using the information at larger  $k$ . Since the FoG effect is still very difficult to reliably model from first principles, the empirical approach we developed in this paper will be useful for correcting the residual FoG effect, or at least making a sanity check of the residual FoG effect.

Recently Masaki et al. (2012) developed a method to generate a mock catalog of the SDSS LRGs based on the abundance matching method, where the central and satellite subhalos in  $N$ -body simulation output are identified as the places hosting LRGs until the number

density of the matched subhalos is similar to that of SDSS LRGs. They nicely showed that the mock catalog fairly well reproduces the SDSS measurements for the satellite LRG fraction, the projected correlation function, the LRG weak lensing, and the redshift-space power spectrum. The mock catalog predicts that some of LRGs in the single-LRG systems are off-centered. Also interestingly, they found that off-centered LRGs in the multiple-LRG halos typically have a velocity dispersion of 500 km/s, which is consistent with our finding. It would be worth further exploring a study to compare the measurement with the mock catalog and the halo model in order to understand the nature of LRGs.

There are some limitations in the FoG correction for the SDSS LRG catalog. First, the statistical accuracy of the LRG-galaxy lensing measurement is limited by the small number density of background galaxies (about  $1.2 \text{ arcmin}^{-2}$  for the SDSS photometric galaxies), and also by the typical SDSS seeing (typically  $1.2''$  FWHM). Second, we lack a good indicator of the halo center for each single LRG system. If deeper imaging data is available, it may help us to identify member galaxies around each LRG and then estimate the richness of each LRG system, e.g. by using optical richness or the number of member galaxies. In addition, since LRGs are selected by a well-tuned color cut, there may be more luminous galaxy(ies) in some of LRG systems, e.g., blue-color brightest cluster galaxy. If such richness information on member galaxies or other luminous galaxies are available, we can use the method in this paper for all the LRG systems by comparing the correlation measurements for the different halo center proxies. Then, we may be able to correct the residual FoG effect more accurately for all the LRG systems. The Subaru HSC survey is planning to have an overlap with the SDSS region, for about 1500 square degrees. The number density of galaxies behind  $z \sim 0.3$  LRGs, usable for the shape measurement analysis, is about  $20 \text{ arcmin}^{-2}$ , a factor of almost 20 larger than for SDSS. Although the area of the HSC survey is about a factor of 7 smaller than that of the SDSS (about  $10000 \text{ deg}^2$ ), the HSC can improve the measurement accuracies by more than a factor of  $\sqrt{20/7} = 1.7$  at each radial bin, due to the additional gain in the lensing efficiency based on the higher mean redshift of source galaxies than in the SDSS. Since LRGs in the 1500 sq. degrees area can be safely considered as a fair, representative sample of LRGs, the HSC survey would improve the accuracy of the FoG correction for the entire SDSS LRG sample, and will more generally increase our understanding of the nature of LRGs and their relation to their host halos. Furthermore, the higher number density of imaging galaxies can also improve the accuracies of the projected cross-correlation measurements.

The deeper depth of an imaging survey such as the HSC survey is also very useful to extend the method of this paper to massive galaxies at higher redshifts, which is being surveyed by the SDSS-III BOSS survey. BOSS has a denser sampling of massive galaxies by a factor of 3-4 compared to the SDSS, so the FoG contamination can be more significant. Again, by having background galaxies around each BOSS galaxy and/or photometric galaxies in the BOSS galaxy redshift range ( $z = [0.4, 0.75]$ ), we can use weak lensing and cross-correlation measurements to observationally explore the nature of those massive red galaxies and to remove the FoG contamination for doing cosmology. These are all crucial in order to reliably use the amplitude and shape information of the galaxy power spectrum in order to constrain the growth rate as well as cosmological parameters such as the neutrino masses.

Our paper demonstrates the complementarity of spectroscopic and imaging surveys for observationally constraining the connection between galaxies and dark matter halos. This is just one example, and there are various synergies available, if the imaging and spectroscopic surveys see the *same* region of the sky (or have at least a sufficiently large overlapping area). This is the case for the SDSS BOSS and the HSC survey, the HSC and PFS surveys, and the Euclid survey. First, as we stressed in this paper, we can measure the galaxy-galaxy lensing or the cross-correlation as a function of the projected radius  $R$  in the comoving unit from the spectroscopic galaxies, rather than the angular separation. The correlations do not mix different scales at different redshifts, and can preserve the same physical radius even if taking a wider redshift slice in the correlation analysis, e.g., the virial radii of halos or the BAO scales. Hence, such correlation functions measured against the projected radii  $R$  yield a measurements of the three-dimensional power spectrum or correlation functions (see Eqs. 9 and 14). This is obvious, but has not been explicitly stressed in the literature. Furthermore, combining the imaging and spectroscopic surveys allows for a reconstruction of galaxy bias functions on large scales as well as a calibration of other systematic errors such as the halo mass, photo- $z$  errors, and shear multiplicative biases (Reyes et al. 2010; Baldauf et al. 2010; Oguri & Takada 2011; Mandelbaum et al. 2012b). Thus various synergies between imaging and spectroscopic surveys need to be more carefully explored in order to attain the full potential of these surveys for deriving the most stringent and robust constraints possible.

## ACKNOWLEDGMENTS

We thank Shirley Ho, Issha Kayo, Surhud More, Beth Reid, Uros Seljak and Kazuhiro Yamamoto for useful discussion and valuable comments. We also acknowledge an anonymous referee for useful and constructive comments that helped improve the manuscript of our paper. CH acknowledges support from a Japan Society for Promotion of Science (JSPS) fellowship green and Grant-in-Aid for Scientific Research from the Ministry of Education, Science, Sports, and Culture, Japan, No. 24740160. RM acknowledges the support of the Department of Energy Early Career Award program for some of the duration of this work. MT greatly thanks Department of Astrophysical Sciences, Princeton University for its warm hospitality during his visit, where this work was done. MT and RM also thank the Aspen Center for Physics and the NSF Grant #1066293 for their warm hospitality, where this work was partly done. DNS and CH acknowledge support from NSF grant AST-0707731 and the NASA AST theory program. DNS thanks the IPMU for its warm hospitality during his visit, where the work was completed. This work is in part supported in part by JSPS Core-to-Core Program ‘‘International Research Network for Dark Energy’’, by Grant-in-Aid for Scientific Research from the JSPS Promotion of Science, by Grant-in-Aid for Scientific Research on Priority Areas No. 467

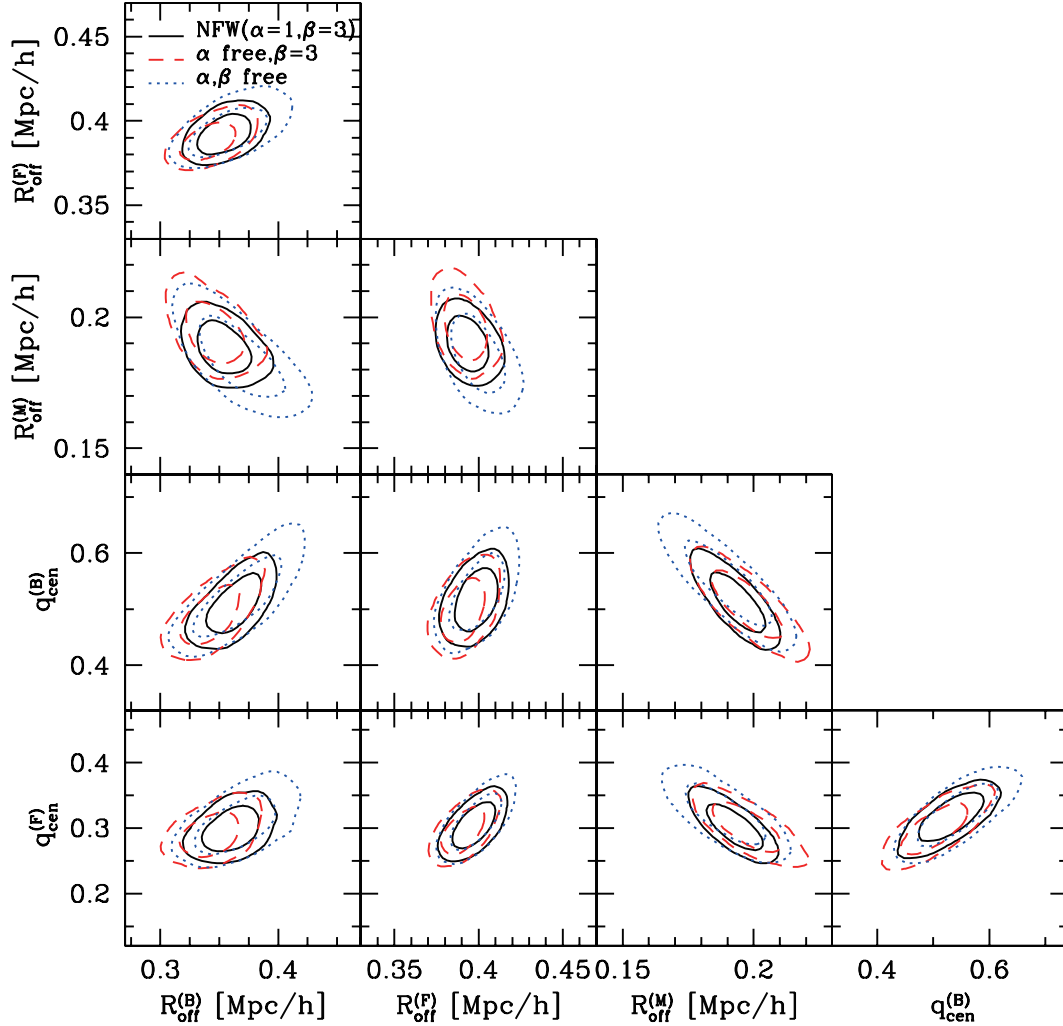


**Figure A1.** Similarly to Fig.7, but the marginalized constraint contours (68 and 95 per cent C.L.) derived from the measured cross-correlations of LRGs with photometric galaxies for the different halo centers (the right panel of Fig.4), where we used the generalized NFW profile,  $n_g(r) \propto 1/[r^\alpha(1+r/r_s)^{\beta-\alpha}]$ , for the radial distribution of photometric galaxies and allow the two parameters  $(\alpha, \beta)$  to freely vary in the model fitting in addition to the set of parameters (Eq. 24). Note that we used the range of  $0.1 \leq R \leq 4$  Mpc/h, and the solid contours are the same as those in Fig.7. The dashed contours are the results when varying only  $\alpha$ , but fixing  $\beta = 3$ . The dotted contours are the results when varying both  $\alpha$  and  $\beta$ , where we employed the priors  $\alpha = [0, 3]$  and  $\beta = [1, 5]$ . The best-fit parameters  $\alpha = 1.4 \pm 0.2$  and  $\beta = 3.3 \pm 0.2$ . The confidence contours are only slightly enlarged for the generalized NFW profile, and the results are consistent with the results obtained by assuming an NFW profile. Thus the results show that the off-center parameters are well constrained, irrespective of the form of the radial profile, by combining the measurements of different centers.

“Probing the Dark Energy through an Extremely Wide & Deep Survey with Subaru Telescope”, by World Premier International Research Center Initiative (WPI Initiative), MEXT, Japan, by the FIRST program “Subaru Measurements of Images and Redshifts (SuMIRE)”, CSTP, Japan, and by the exchange program between JSPS and DFG.

## APPENDIX A: IMPACT OF AN NFW PROFILE ASSUMPTION ON THE OFF-CENTERING PARAMETERS FROM THE LRG-GALAXY CROSS-CORRELATION

One of the main uncertainties in the off-center constraints we derived from the measured cross-correlation functions of LRGs with photometric galaxies is the assumption of an NFW profile for the photometric galaxies. Here we study how the off-centering parameters are changed by relaxing the NFW assumption. To study this, we assume that the radial distribution of photometric galaxies follows a generalized NFW profile given as  $n_g(r) \propto 1/[r^\alpha(1+r/r_s)^{\beta-\alpha}]$ , where  $r_s$  is the scale radius given in terms of the virial radius and the halo concentration as  $r_s = r_{180b}/c_{180b}$ . In the model fitting, we allow the two parameters  $(\alpha, \beta)$  to freely vary, in addition to the set of free parameters in Eq. (24). We employ flat priors on the new parameters as  $\alpha = [0, 3]$  and  $\beta = [1, 5]$ , where the profile with  $\alpha = 1$  and  $\beta = 3$  corresponds to an NFW profile.

Fig.A1 shows the marginalized confidence regions for the off-centering parameters, similarly to Fig.7, where we used the cross-

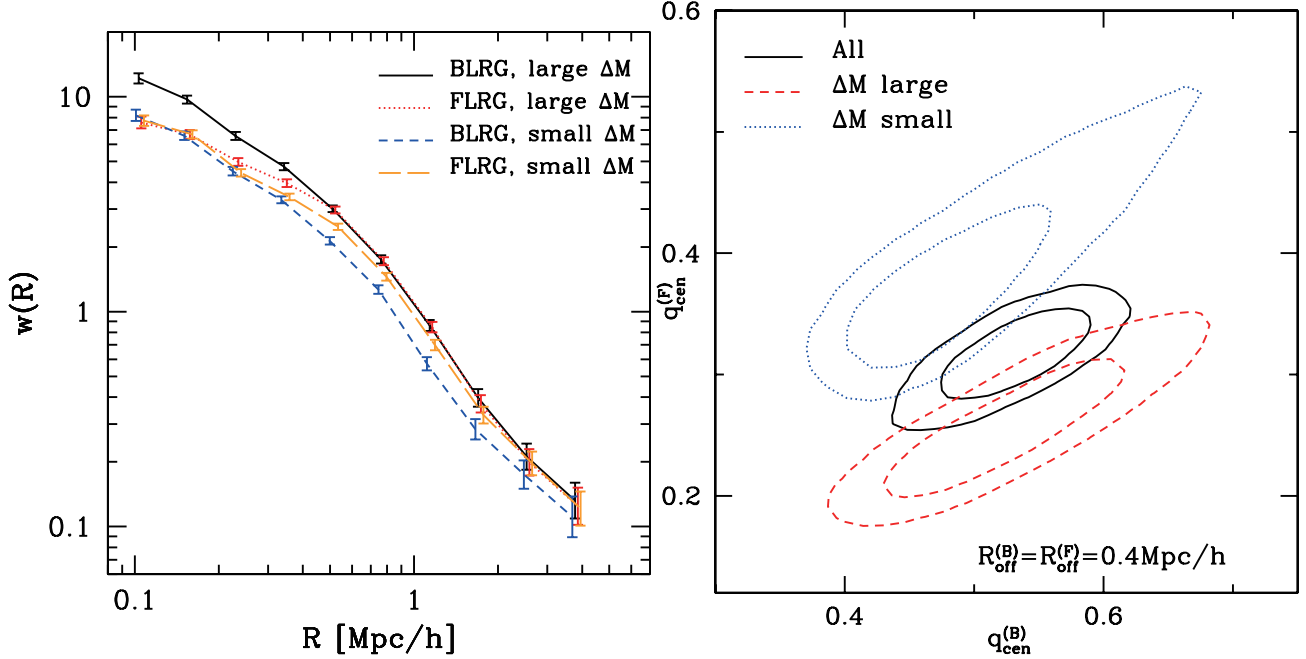


**Figure B1.** *Left panel:* the cross-correlation functions of the BLRG or FLRG position with the photometric galaxies, for the two subsamples of the multiple-LRG systems, where the multiple-LRG systems are divided into halves. One subsample is defined by the systems which have the larger magnitude difference between BLRG and FRLG than the median (larger  $\Delta M$ ), while the other contains the remaining systems, those with the smaller magnitude difference (smaller  $\Delta M$ ). For each subsample, we measured the cross-correlations for the BLRG or FLRG centers as indicated by the legend. Note that the correlation amplitudes are not reliable due to the dilution effect caused by photo- $z$  errors. *Right panel:* the best-fit off-centering parameters obtained from each sub-sample. Since we cannot obtain sufficiently tight constraints on the parameters due to insufficient statistical power, we fixed the typical off-centering radius to  $R = 400$  kpc/h for both the BLRG and FLRG centers, and constrained the fraction of central BLRGs or FLRGs,  $q_{\text{cen}}^{\text{BLRG}}$  or  $q_{\text{cen}}^{\text{FLRG}}$ . The fraction of the central BLRGs is not different for the two subsamples, but the fraction of the central FLRGs is smaller for the subsample with the larger magnitude difference.

correlations for the different centers in the range of  $0.1 < R < 4$  Mpc/h. The dashed contours are the results when we allow only  $\alpha$  to freely vary, and the dotted contours are the results when both  $\alpha$  and  $\beta$  are freely varied. The best-fit parameters are  $\alpha = 1.4 \pm 0.2$  and  $\beta = 3.3 \pm 0.2$  for the latter model, and the best-fit model is consistent with an NFW profile. These results are compared to the solid contours, which are the results in Fig.7. The figure shows that, even if allowing a more generalized profile, each of the off-centering parameters is well constrained and the confidence region is only slightly enlarged by adding the two parameters. Thus the degeneracy between the off-centering parameters and the profile parameters is efficiently broken by comparing the cross-correlations for the different choices of halo centers. As we discussed in the main text (see Section 4), the off-centering parameters for the single-LRG systems are significantly degraded if relaxing the NFW assumption, because it does not allow for comparison between the measurements of different centers (only the single LRG itself can be taken as the center in the correlation calculation): we found  $q_{\text{cen}} = 0.76 \pm 0.06$  and  $R_{\text{off}} = (0.26 \pm 0.03)$  Mpc/h for the NFW assumption, while these constraints became  $q_{\text{cen}} = 0.79 \pm 0.08$  and  $R_{\text{off}} = 0.26 \pm 0.15$  Mpc/h for the generalized NFW profile. Thus the constraints on the offset radius are considerably weaker.

## APPENDIX B: DEPENDENCE OF THE OFF-CENTERING EFFECTS ON THE MAGNITUDE DIFFERENCE BETWEEN BLRG AND FLRG

We found that some BLRGs in the multiple-LRG systems are satellite galaxies. As shown in Fig.2, the BLRG in some systems is brighter than FLRG by only a few tenths of a magnitude, implying that BLRG and FLRG are not so different. Given this fact, one might consider that satellite BLRGs are mainly from such multiple-LRG systems where the FLRG is instead a central galaxy and the BLRG is a satellite. On the other hand, for systems where the BLRG and FLRG luminosities are significantly different, the BLRG may have a higher chance to be central. In this appendix, we study this possibility by dividing the multiple-LRG systems into halved subsamples in terms of the magnitude difference between BLRG and FLRG in each system. One halved subsample contains the systems for which the BLRG and FLRG have a smaller magnitude difference than the median (the “small  $\Delta M$ ” subsample), while the other subsample contains the remaining systems (the larger “ $\Delta M$ ”).

The left panel of Fig.B1 shows the measured cross-correlations for the halved subsamples, using either BLRG or FLRG centers. The cross-correlations for the different subsamples and centers differ from each other, especially in their amplitudes. However, as we stressed in Section 2.4, we cannot directly compare the correlation amplitudes because the amplitude suffers from a dilution due to photo- $z$  errors. Instead we need to use the shape of the correlation function to infer the off-centering effects. By fitting the halo model to the cross-correlations, we



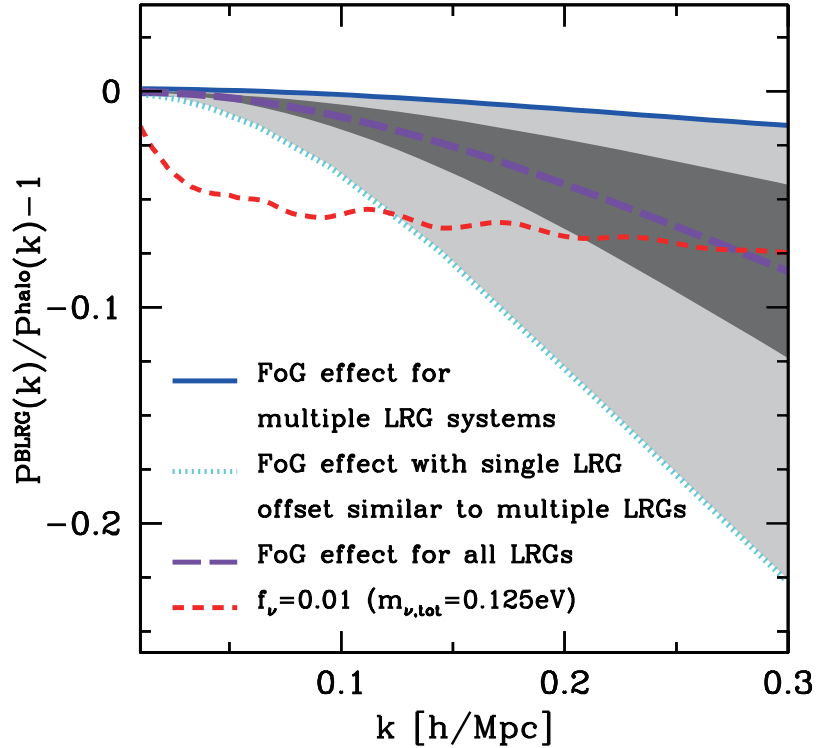


**Figure C1.** Similarly to Fig.11, but the residual FoG effect implied from the off-center parameters constrained from the LRG-galaxy weak lensing for the single-LRG systems (the left panel of Fig.10).

estimate the off-centering parameters. However, due to the insufficient statistical accuracies of the halved subsample, we were not able to obtain tight constraints on the parameters, after marginalizing over other parameters. Hence, in the right panel, we show the constraints on the fractions of central BLRGs or FLRGs for each of the two subsamples when fixing the off-centering radius to  $0.4 \text{ Mpc}/h$ , the best-fit value for all the multiple-LRG systems. The plot shows that the fraction of central BLRGs is similar for the two subsamples,  $q_{\text{cen}}^{\text{BLRG}} \simeq 0.5$ , but the fraction of central FLRGs is higher for the subsample with the smaller magnitude difference between BLRG and FLRG than the other subsample, supporting the hypothesis that the FLRG is not so different from the BLRG, and the FLRG is instead a central galaxy in the subsample.

### APPENDIX C: IMPLICATION FOR THE RESIDUAL FOG EFFECT IN THE LRG POWER SPECTRUM FROM THE LRG-GALAXY WEAK LENSING

In Section 4, we discussed a possible residual FoG effect in the LRG redshift-space power spectrum arising from the off-centering effects of LRGs. To discuss this effect, we used the cross-correlation measurement for the single-LRG systems, and the constraints on off-centering parameters to infer a possible FoG effect in Fig.11. For completeness, Fig.C1 shows the residual FoG effect implied from the off-centering of LRG-galaxy weak lensing (assuming the NFW profile). Due to the smaller signal-to-noise ratio for the LRG-galaxy compared to the galaxy cross-correlation, the off-centering parameters are not well constrained;  $q_{\text{cen}} = 0.76 \pm 0.18$  and  $R_{\text{off}} = 0.38 \pm 0.25 \text{ Mpc}/h$  for single-LRG systems and  $q_{\text{cen}} = 0.63 \pm 0.21$  and  $R_{\text{off}} = 0.44 \pm 0.22 \text{ Mpc}/h$  for multiple-LRG systems. The dark shaded region in Fig.C1 shows the implied range of residual FoG effect, which is wider than that in Fig. 11. Nevertheless, we should emphasize that the FoG effects in Figs. 11 and C1 are consistent with each other within the error bars.

### REFERENCES

- Abazajian K. N. et al., 2009a, ApJS, 182, 543
- Abazajian K. N. et al., 2009b, ApJS, 182, 543
- Aihara H. et al., 2011, ApJS, 193, 29
- Albrecht A. et al., 2006, arXiv:astro-ph/0609591
- Anderson L. et al., 2012, arXiv:1203.6594
- Baldauf T., Smith R. E., Seljak U., Mandelbaum R., 2010, Phys. Rev. D, 81, 063531
- Berlind A. A., Weinberg D. H., 2002, ApJ, 575, 587

- Blake C., et al., 2011, arXiv:1104.2948
- Chen J., 2009, *A.&Ap.*, 494, 867
- Cole S., et al., 2005, *ApJ*, 362, 505
- Davis M., Huchra J., 1982, *ApJ*, 254, 437
- Dawson K. S. et al., 2012, arXiv:1208.0022
- de Lapparent V., Geller M. J., Huchra J. P., 1986, *ApJ*, 302, L1
- Eisenstein D. J. et al., 2001a, *AJ*, 122, 2267
- Eisenstein D. J., Hu W., Tegmark M., 1999, *ApJ*, 518, 2
- Eisenstein D. J., et al., 2001b, *AJ*, 122, 2267
- Eisenstein D. J., et al., 2005, *ApJ*, 633, 560
- Ellis R. et al., 2012, arXiv:1206.0737
- Feldman H. A., Kaiser N., Peacock J. A., 1994, *ApJ*, 426, 23
- Feldmann R. et al., 2006, *MNRAS*, 372, 565
- Fukugita M., Ichikawa T., Gunn J. E., Doi M., Shimasaku K., Schneider D. P., 1996, *AJ*, 111, 1748
- George M. R. et al., 2012, arXiv:1205.4262
- Gunn J. E. et al., 1998, *AJ*, 116, 3040
- Guo Q., Cole S., Eke V., Frenk C., 2012, *MNRAS*, 427, 428
- Guzik J., Jain B., Takada M., 2010, *Phys. Rev. D*, 81, 023503
- Guzzo L., et al., 2008, *Nature*, 451, 541
- Hamilton A. J. S., 1998, in *Astrophysics and Space Science Library*, Vol. 231, *The Evolving Universe*, D. Hamilton, ed., pp. 185–+
- Hartlap J., Simon P., Schneider P., 2007, *A.&Ap.*, 464, 399
- Hikage C., Takada M., Spergel D. N., 2012, *MNRAS*, 419, 3457
- Hirata C., Seljak U., 2003, *MNRAS*, 343, 459
- Hirata C. M. et al., 2004, *MNRAS*, 353, 529
- Hogg D. W., Finkbeiner D. P., Schlegel D. J., Gunn J. E., 2001, *AJ*, 122, 2129
- Ivezić Ž. et al., 2004, *Astronomische Nachrichten*, 325, 583
- Jackson J. C., 1972, *MNRAS*, 156, 1P
- Johnston D. E., et al., 2007, arXiv:0709.1159
- Kaiser N., 1987, *MNRAS*, 227, 1
- Kazin E. A. et al., 2010, *ApJ*, 710, 1444
- Kirshner R. P., Oemler, Jr. A., Schechter P. L., Shectman S. A., 1987, *ApJ*, 314, 493
- Komatsu E. et al., 2011, *ApJS*, 192, 18
- Komatsu E., et al., 2009, *Astropys.J.Suppl.*, 180, 330
- Leauthaud A., et al., 2010, *ApJ*, 709, 97
- Limber D. N., 1954, *ApJ*, 119, 655
- LSST Science Collaborations, Abell P. A., et al., 2009, arXiv:0912.0201
- Lupton R. H., Gunn J. E., Ivezić Z., Knapp G. R., Kent S., Yasuda N., 2001, in *ASP Conf. Ser. 238: Astronomical Data Analysis Software and Systems X*, pp. 269–+
- Mandelbaum R., Hirata C. M., Leauthaud A., Massey R. J., Rhodes J., 2012a, *MNRAS*, 420, 1518
- Mandelbaum R. et al., 2005, *MNRAS*, 361, 1287
- Mandelbaum R., Seljak U., Cool R. J., Blanton M., Hirata C. M., Brinkmann J., 2006a, *MNRAS*, 372, 758
- Mandelbaum R., Seljak U., Kauffmann G., Hirata C. M., Brinkmann J., 2006b, *MNRAS*, 368, 715
- Mandelbaum R., Slosar A., Baldauf T., Seljak U., Hirata C. M., Nakajima R., Reyes R., Smith R. E., 2012b, arXiv:1207.1120
- Masaki S., Hikage C., Takada M., Spergel D. N., Sugiyama N., 2012, arXiv:1211.7077
- Miyazaki S. et al., 2006, in *Society of Photo-Optical Instrumentation Engineers (SPIE) Conference Series*, Vol. 6269, *Society of Photo-Optical Instrumentation Engineers (SPIE) Conference Series*
- More S., van den Bosch F. C., Cacciato M., Mo H. J., Yang X., Li R., 2009, *MNRAS*, 392, 801
- Nakajima R., Mandelbaum R., Seljak U., Cohn J. D., Reyes R., Cool R., 2012, *MNRAS*, 420, 3240
- Navarro J. F., Frenk C. S., White S. D. M., 1996, *ApJ*, 462, 563
- Newman J. A., 2008, *ApJ*, 684, 88
- Oguri M., Takada M., 2011, *Phys. Rev. D*, 83, 023008
- Okabe N., Takada M., Umetsu K., Futamase T., Smith G. P., 2010, *Publ. Soc. Astron. Japan*, 62, 811
- Padmanabhan N. et al., 2008, *ApJ*, 674, 1217
- Peacock J. A., Dodds S. J., 1994, *MNRAS*, 267, 1020
- Peacock J. A., Schneider P., Efstathiou G., Ellis J. R., Leibundgut B., Lilly S. J., Mellier Y., 2006, *ESA-ESO Working Group on "Fundamental Cosmology"*. Tech. rep.
- Peacock J. A., et al., 2001, *Nature*, 410, 169

- Percival W. J., Verde L., Peacock J. A., 2004, MNRAS, 347, 645  
Percival W. J., White M., 2009, MNRAS, 393, 297  
Percival W. J., et al., 2007, ApJ, 657, 51  
Pier J. R., Munn J. A., Hindsley R. B., Hennessy G. S., Kent S. M., Lupton R. H., Ivezić Ž., 2003, AJ, 125, 1559  
Reid B. A. et al., 2012, arXiv:1203.6641  
Reid B. A., Spergel D. N., 2009, ApJ, 698, 143  
Reid B. A., Spergel D. N., Bode P., 2009, ApJ, 702, 249  
Reid B. A., et al., 2010, ApJ, 404, 60  
Reyes R., Mandelbaum R., Gunn J. E., Nakajima R., Seljak U., Hirata C. M., 2011, arXiv:1110.4107  
Reyes R., Mandelbaum R., Seljak U., Baldauf T., Gunn J. E., Lombriser L., Smith R. E., 2010, Nature, 464, 256  
Richards G. T. et al., 2002, AJ, 123, 2945  
Ross N. P., et al., 2007, MNRAS, 381, 573  
Ross N. P., et al., 2008, MNRAS, 387, 1323  
Schlegel D. J., et al., 2009, arXiv:0904.0468  
Schulz A. E., Mandelbaum R., Padmanabhan N., 2010, MNRAS, 408, 1463  
Soccimarro R., 2004, Phys. Rev. D, 70, 083007  
Sehgal N. et al., 2012, arXiv:1205.2369  
Seljak U., 2001, MNRAS, 325, 1359  
Sheldon E. S., et al., 2009, ApJ, 703, 2217  
Sheth R., Tormen G., 1999, MNRAS, 308, 119  
Skibba R. A., van den Bosch F. C., Yang X., More S., Mo H., Fontanot F., 2011, MNRAS, 410, 417  
Smith J. A. et al., 2002, AJ, 123, 2121  
Song Y., Kayo I., 2010, MNRAS, 407, 1123  
Song Y., Percival W. J., 2009, JCAP, 10, 4  
Strauss M. A. et al., 2002, AJ, 124, 1810  
Takada M., Jain B., 2003, MNRAS, 340, 580  
Tang J., Kayo I., Takada M., 2011, MNRAS, 416, 2291  
Tegmark M., et al., 2004, ApJ, 606, 702  
Tucker D. L. et al., 2006, Astronomische Nachrichten, 327, 821  
Wake D. A., et al., 2008, MNRAS, 387, 1045  
Wang Y., 2008, JCAP, 5, 21  
Wang Y., Spergel D. N., Strauss M. A., 1999, ApJ, 510, 20  
White M., 2001, MNRAS, 321, 1  
White M., Song Y., Percival W. J., 2009, MNRAS, 397, 1348  
White M., et al., 2011, ApJ, 728, 126  
Yamamoto K., Nakamura G., Hütsi G., Narikawa T., Sato T., 2010, Phys. Rev. D, 81, 103517  
York D. G. et al., 2000a, AJ, 120, 1579  
York D. G., et al., 2000b, Astron. J., 120, 1579  
Zhang P., Liguori M., Bean R., Dodelson S., 2007, Physical Review Letters, 99, 141302  
Zheng Z., Zehavi I., Eisenstein D. J., Weinberg D. H., Jing Y. P., 2009, ApJ, 707, 554